CLM-P71

United Kingdom Atomic Energy Authority

RESEARCH GROUP

Preprint

FAUST I
A HARDCORE DISCHARGE STABILITY EXPERIMENT

K. L. AITKEN
K. J. HOPKINS
R. J. BICKERTON
R. A. HARDCASTLE
P. REYNOLDS

Culham Laboratory,

Culham, Abingdon, Berkshire

1965

UNCLASSIFIED
(Approved for Publication)

CLM-P 71

FAUST 1 – A HARDCORE DISCHARGE STABILITY EXPERIMENT

by

K.L. Aitken
K.J. Hopkins
R.J. Bickerton
R.A. Hardcastle
P. Reynolds

(Submitted for publication in Nuclear Fusion)

U.K.A.E.A. Research Group,
Culham Laboratory,
Nr. Abingdon,
Berks.

January, 1965 (C/18 IMG)

A B S T R A C T

A hardcore discharge stability experiment is described in which the final configuration is obtained by the radial inward collapse of the plasma sheath from the wall of the tube. By varying the initial conditions an axial field of arbitrary sign can be trapped within the annular plasma column. The construction and mode of operation of the apparatus is fully described.

The gas currents were of the order of 50 kA, with rod currents of 120 kA so that the current in the gas was less than half that in the rod at all times. The general behaviour of the discharge was examined and the effect of pressure, preionization and trapped axial field studied. A detailed examination was made of a representative set of conditions with electric, magnetic and double Langmuir probes. These measurements, together with quantities derived from them, are discussed and the derived values of electron temperature and kinetic pressure are compared with the directly measured values. The validity of the pressure balance analysis is considered in the light of these results.

The discharge, without trapped axial field, showed a high degree of reproducibility and the observed fluctuations were of low amplitude ($< 10\%$) and low frequency ($\sim$ 500 kc/s) in both electric and magnetic field as well as in particle density. The latter showed a well-defined annular sheath until late in the half-cycle and the radial profiles of azimuthal and axial current densities, kinetic pressure, temperature, and particle density show good agreement. With trapped axial field, however, the discharge showed a reduction in stability especially with trapped reverse field which introduces a null in the total axial field. Even with these, the most unstable conditions, the fluctuations were still relatively small ($< 20\%$) and of low frequency ($\sim$ 1 Mc/s). The stability of the discharge is quantitatively compared with stability theory and the results discussed.

CONTENTS

INTRODUCTION

The aim of the FAUST 1 (fast axial unpinch stability tube) experiment was to study the stability of a linear hardcore discharge under a variety of magnetic field configurations. The field configurations of interest were:

(a) A hardcore discharge in which the current through the gas is only slightly less than that through the central rod. Inside the plasma column there is mainly a B_θ field; outside the column there is mainly a B_z field and the plasma is compressed between these two fields.

(b) A configuration where the plasma current in the axial direction is considerably less than that through the central rod. There is then a B_θ field both inside and outside the plasma column. Such an arrangement of fields is theoretically more stable than (a) with respect to the resistive 'tearing mode' instability[1,2]

(c) A configuration in which a B_z field exists inside the plasma column as well as outside it. The field inside the column can be either in the same or the opposite direction as that outside. It was thought that the change in stability produced by such a B_z field configuration might throw some light on the instability mechanism[3].

The FAUST 1 apparatus enables comparisons between (a), (b) and (c) to be made in the same discharge tube.

Arrangements (a) and (b) can be produced by means of the conventional inverse pinch discharge in which the gas discharge starts near a central rod sheathed in insulating material, and expands radially towards the outer wall of the tube until it is brought to rest by a B_z field compressed between the expanding plasma and the metal outer sheath of the discharge tube.

To obtain arrangement (c) however, a different approach must be adopted. This is because any B_z field present in the tube originally is 'swept out' by the discharge as it expands from the rod. To include B_z field inside the plasma column the hardcore discharge must therefore be formed by pinching a plasma column on to

an initially present B_z field. FAUST 1 enables this to be done by compressing the plasma cylinder by means of a rising B_z field produced by a thetatron type coil, on to a previously established B_θ field and, if required, on to an initially present B_z field also. In operation it is similar to a linear section of a levitron tube.

The FAUST 1 configuration set up by the collapse of the current layer from the wall is known to be inherently more stable[4] than that in the conventional hardcore where the plasma expands from the rod.

In the present work the general behaviour of the discharge is described, as is the effect on it of varying pressure, degree of pre-ionization etc. A detailed experimental investigation of a selected set of conditions is described which was made in order to examine the fine-scale behaviour of the discharge and to study the stability of the system.

PRINCIPLE OF OPERATION OF FAUST 1 APPARATUS

Fig.1 shows a schematic arrangement of the apparatus used and Fig.2 an indication of the currents flowing in various parts of the circuit.

Neglecting for the moment the slow B_z circuit let us consider the remaining circuits. The B_θ capacitor bank supplies current to the hardcore and this current returns via conductors on the outside of the quartz vacuum tube. (Straps rather than a complete shell are used to allow penetration into the tube of the fast B_z flux from the single turn winding). Fig.2(b) shows the waveform of the rod current when no gas current flows. At peak rod current (400 μsec), the fast B_z capacitor bank is fired, which causes current to flow in the single turn B_z winding with a rise-time of 14 μsec, Fig.2(c). An azimuthal electric field is set up in the gas, which causes an azimuthal current discharge to be initiated near the outer wall of the discharge tube. This thetatron-like discharge now pinches towards the hardcore, but in moving through the already established B_θ field it polarizes longitudinally and breakdown occurs between the ends of the discharge cylinder and the electrodes.

There are now two circuits containing B_θ magnetic flux which are 'short-circuited'.

(a) Circuit ABCD. The B_θ flux in this circuit is conserved. This means that as the cylinder pinches inwards the B_θ field inside this region increases, which is brought about by an increase in rod current (upper oscillatory wave-form of 2(b)).

(b) Circuit BEFC. This is also a short circuit, since before the fast B_z circuit is fired, the B_θ circuit is clamped. The B_θ flux between the discharge (at the instant of breakdown to the electrode) and the return current straps, plus the flux in the external inductor is conserved. If the wall of the vacuum vessel is thin, the flux to be conserved is correspondingly small, and the gas current I_G, after substantial pinching has occurred, will almost equal the rod current I_R but will be in the opposite direction. The strap current I_S is then almost zero.

In this way current conditions similar to those in the normal inverse pinch discharge are obtained. If, on the other hand, the external inductance is not small compared with the other inductances in the circuit, then it will contain an appreciable amount of flux, and the current in the return current straps does not fall almost to zero, but takes on a value depending on the size of the external inductance and the radial position of the current layer in the tube (lower curve of 2(b)).

In the absence of any initially applied B_z field the collapsing current sheet comes to rest when the external driving B_z field is balanced by the compressed internal B_θ field. Compared with the normal pinch discharge the roles of B_θ and B_z are reversed in this system.

Assuming that there is complete trapping of the B_θ flux, the relation between the initial rod current I_{R1} and the rod current I_{R2} after the current channel has been compressed to a radius R_2 is given by:

$$\frac{I_{R2}}{I_{R1}} = \frac{\log_e \frac{R_1}{R_o}}{\log_e \frac{R_2}{R_o}}$$

where R_o is the radius of the hardcore and R_1 is the radius at which axial breakdown of the gas first occurs. The relation between the rod current I_{R2} and the axial gas current I_G flowing when the channel has reached a radius R_2 is given by

$$\frac{I_{R2}}{I_G} = \frac{2\ell \log_e \frac{R_s}{R_2} + L}{2\ell \left[\log_e \frac{R_s}{R_2} - \log_e \frac{R_s}{R_1} \frac{\log_e \frac{R_2}{R_o}}{\log_e \frac{R_1}{R_o}} \right] + L \left[1 - \frac{\log_e \frac{R_2}{R_o}}{\log_e \frac{R_1}{R_o}} \right]}$$

where R_s is the radius at which the return current straps are situated and L is the external inductance in the circuit (in e.m.u.) and ℓ is the interelectrode spacing in cms.

For the conditions of the experiment $\frac{I_{R2}}{I_G}$ could be varied between 1.2 and 2.5 approximately.

CONSTRUCTION AND OPERATION

Details of the construction of the apparatus are shown in Fig.3. Fig.4 is a photograph of the completed apparatus. The vacuum vessel was a fused quartz tube, 30 cm bore with stainless steel electrodes at each end. These electrodes were joined electrically by a copper rod of 2.5 cm diameter, which was uninsulated. The tube was pumped by a 6" oil diffusion pump fitted with a liquid nitrogen trap. The range of operating pressures of the system was 5 - 100 mTorr and was achieved by admitting gas through the lower electrode via a needle valve, with the pump throttled by a baffle valve. Under these conditions of slow pumping speed the background gas pressure in the tube was 5×10^{-5} mTorr so that the percentage impurity in the gas in the tube was $\sim$ 0.3%. The quartz tube was sealed to the lower electrode by an indium wire gasket which was replaced in the course of the investigations by a silicon rubber O-ring, and to the upper electrode by an indium wire

gasket. Both seals were concealed from the discharge.

To allow for the differential expansion of the copper rod and the quartz tube, and also to allow for the expansion of the rod under the action of the magnetic forces, the top electrode is connected to the return current conductors by flexible connectors. The 16 return conductors are made of 2.5 cm wide copper strips, equally spaced around the circumference of the tube which gives an approximately uniform B_θ field at the inner surface of the quartz tube and allows the entry of the fast rising B_z field from the single turn winding.

The central rod and return conductors are connected to the 6 kV capacitor bank via a large pulse transformer which steps down the voltage to the tube by 8 times, in order to prevent gas breakdown during the establishment of the initial azimuthal magnetic field.

The pulse transformer is a large ring core of mean diameter 86 cm and cross sectional area 1125 cm^2 wound with closely coupled primary and secondary windings. The secondary winding consists of a single turn copper sheet fitting over the primary turns. In this way the external inductance L introduced by the transformer is only 6 $m\mu H$ referred to the secondary circuit. A larger value of L to control the ratio of hardcore to gas current can be obtained by inserting a series inductor on the primary side of the transformer.

The fast B_z winding is a single turn of copper sheet, 0.15 cm thickness 35 cm diameter, closely wound on top of the return conductors and insulated from them by a sheet of polythene. This winding does not extend over the full inter-electrode distance, leaving a 5 cm gap at each end for the B_z flux to escape from the tube, since the rise-time of the B_z is too fast to allow it to penetrate the electrodes. Connection of the fast B_z loop to the 15 kV capacitor bank is by means of 60 coaxial cables from 10 pressurised spark gaps. The external inductance is such that 2/3 of the capacitor voltage appears across the terminals of the B_z loop.

The slow B_z winding is a conventionally wound solenoid. The inside diameter

of 63 cm is much larger than that of the fast winding to allow room for the return B_z flux of the fast winding to pass inside the slow winding. A stainless steel sheath on the inside of the slow winding ensures that there is no appreciable voltage induced by the fast B_z flux into the slow winding. The stainless steel sheath is 3 mm thick so that the slow B_z field can easily penetrate it.

When the tube was first set up difficulty was experienced with the breakdown of the gas on the first half-cycle of the fast B_z, particularly when there was an added slow B_z field which connected the discharge to the electrodes. Four igniter pins were therefore fitted in each electrode and these enable the gas to break down satisfactorily on the first half-cycle. The power supplies for these igniter pins are described below (see 'Effect of Igniters'); the construction of the pins is shown in Fig.5.

The vacuum vessel was drilled with several holes which enabled magnetic and double probes (see below) to be inserted diametrically opposite each other at a point midway between the electrodes and also within 2 cm of the electrode surface. There were also wall coils, to measure the external B_θ and B_z fields, attached to the inside of the return current conductors, and a Rogowski coil around one of these conductors.

DIAGNOSTIC EQUIPMENT USED

Measurements were made of:

(a) Magnetic fields. Vacuum profiles were measured using a Hall effect probe[5]; and discharge profiles using conventional single and multiple pick-up coil magnetic probes with an R-C integrator circuit. These probes were used inside a quartz-walled tube and were not exposed to the discharge.

(b) Currents flowing in the external circuit. These were measured using a Rogowski coil and R-C integrator circuit.

(c) Particle densities and electron temperature. Biassed double Langmuir probes were used for these measurements. The construction is indicated in

Fig.6. The electrodes of 0.5 mm diameter platinum wire, were enclosed in 1 mm o.d. ceramic tubes which were mounted parallel to and in the end of the body of the probe which was of 6 mm o.d. ceramic tube. The latter contained an electrostatic screen of brass tubing. For normal operation these probes were operated with bias values between -36 V and +36 V but before any measurements were made they were conditioned by running about 10 shots with a probe bias of 120 V. In effect this discharge-cleaned the electrode surface and was found to be necessary if the tube had not fired for more than an hour or so. The recording oscilloscope was isolated from these probes by a 10 Mc/s pulse transformer.

(d) The axial and azimuthal components of electric field - using the probes described in (c) above without the bias voltage supply. Transformers were again used for voltage isolation.

THE DISCHARGE CONDITIONS INVESTIGATED

THE OPERATIONAL VALUES USED

The initial rod current was typically 100 kA which rose to a maximum of 120 kA at a time 5 μsec after the B_z was fired. At this time the axial gas current was 55 kA with the remaining 65 kA returning externally. The driving B_z field rose to 3 kG at 15 μsec, and the plasma equilibrium position (radius 7 cm) was reached in approximately 10 μsec. There was also provision for a vacuum B_z field, maximum value 4 kG, rising in 80 msec and therefore constant for the duration of the discharge cycle.

THE DISCHARGE BEHAVIOUR - GENERAL

BREAKDOWN

The degree of breakdown was judged either by the exclusion of fast B_z from the hardcore region (which depends on the formation and temperature of the sheath) or by the change in the external current carried by the straps (which reflects the growth of axial gas current by virtue of successful B_θ field trapping).

Fig.7 shows good and bad breakdown conditions. The main influence on breakdown was the pressure. Fig.8 shows, in the dotted curve, the decrease in gas current below 60 mTorr; note that at 20 mTorr the tube virtually does not fire. The full curve shows the usefulness of the igniter pins which were put in each electrode to promote breakdown.

EFFECT OF IGNITERS

The igniter system consisted of four pins in each electrode, spaced at 90^{o} and at a large radius (12 cm). The construction is indicated in Fig.5 and briefly they consisted of a copper rod 3 mm diameter extending approximately 6 cm from the electrode surface, and clad in a quartz tube, except for the last cm or so. The design was not critical, and the long tracking path was broken down at voltages above 5 kV at operating pressures. Two igniter supplies were used: 15 kV, 0.11 joules per pin or 8 kV, 32 joules per pin, having periods of about 1 μsec and 50 μsec respectively. The upper curve in Fig.8 was obtained using the 15 kV set only.

It was found that the higher voltage igniters were superior at pressures below 15 mTorr; above this, the more energetic ones were marginally better, in terms of B_z exclusion. The effect of the igniters was independent of the delay in firing the fast B_z circuit: for up to 100 μsec for the 15 kV case and 400 μsec for the 8 kV one. It was decided to use both circuits, connecting two of the four pins in each electrode to each circuit. The 8 kV igniters were fired 10 μsec after the 15 kV and 50 μsec before the fast B_z. In this way, efficient breakdown was obtainable at pressures down to 10 mTorr.

The marginal differences observed between the two igniter systems used, which were of widely differing energies, shows that very little pre-ionization was required to produce adequate breakdown. This is confirmed by the unimportance of the delay between the igniters firing and the firing of the main discharge.

EFFECT OF PRESSURE

Fig.8 shows that even at 60 mTorr, the breakdown is much improved by the

igniters: without igniters the tube will not fire below 20 mTorr, but with igniters the minimum pressure is brought down to less than 5 mTorr, and at 15 mTorr the breakdown is still very good. With igniters and considering the B_z exclusion, the breakdown improves as the pressure is reduced, until it becomes uncertain at about 10 mTorr. At 15 mTorr, the B_z near the hardcore at gas current maximum is $\frac{1}{6}$ of the applied B_z, whilst at 60 mTorr it is $\frac{1}{2}$. This behaviour is compatible with a more rapidly ionized and heated plasma near the outer wall in the lower pressure case. Pressures near to 15 mTorr were generally used as this represented an optimum region.

Without igniters a reduction in pressure produces a decrease in B_z exclusion. At 60 mTorr the diffused field is $\frac{2}{3}$ that applied and this fraction increases as the pressure decreases.

Near the pressure at which the tube fails to fire, delays of 1 - 5 μsec have been observed to occur before breakdown. During this period a vacuum magnetic field configuration is obtained.

SHEATH BEHAVIOUR

Under typical operating conditions, the sheath formed at a radius of 14 cm, and collapsed at roughly 1 cm/μsec for the first 5 μsec, reaching r = 11 cm and then slowing down to reach r = 8 cm after 10 μsec. The final equilibrium position of r = 7 cm was reached between 10 and 12 μsec. The sheath was approximately 2.5 cm thick for the first 20 μsec, diffusion being very small, and the average current densities were of the order of 500 A/cm^2.

FIELD TRAPPING

In collapsing from r = 14 cm to r = 7 cm, with perfect B_θ trapping it would be expected that the rod current would increase by the factor 1.4. In fact the increase is slightly less than 1.2, from 100 to 120 kA.

Since the diffusion rate through the sheath (see below under 'Field Diffusion') is insufficient to account for this it must be assumed that the B_θ flux escaped around the ends of the plasma shell; a 20% loss would explain the result. This

has the effect of reducing the gas current, and such behaviour would imply a poorly conducting shell near the electrodes. In fact the measured temperature and density were not much reduced at the electrode, and the axial electric field E_z at 2 cm from the electrode was only double that at the tube centre (10 V/cm). The poor trapping of B_θ may therefore also be due to late breakdown of the gas in the axial direction.

A further feature of the discharge behaviour was the difference in axial gas current between the centre and electrode regions. From an analysis of the rB_θ profiles (Fig.14), an initial hardcore current of 100 kA would rise to about 118 kA, while the corresponding axial gas currents were 55 kA and 35 kA at centre and electrode respectively. This introduces the possibility of a current which circulates from the sheath: leaving the sheath near one electrode either to flow co-axially in the sheath-wall interspace and rejoin the sheath near the other electrode or leaving the sheath to flow into the uninsulated hardcore near one electrode and flowing from the hardcore back into the sheath again near the other electrode (Fig.9). Magnetic and double probe measurements in the central region should show the presence of any circulating currents between the sheath and the wall, while a current circulating from the hardcore should show up as a difference in hardcore currents at the centre and at the electrode. None of the measurements made point to the presence of either of these currents. The possibility of a spurious pick-up effect due to measurements being made very close to the electrode surface cannot be ruled out.

The trapping of the B_z field is practically as expected. Within the first 4 μsec, a certain amount of B_z is present near the rod, and the sheath implosion compresses this in roughly the correct geometrical ratio.

FIELD DIFFUSION

Axial Field Diffusion

As distinct from the compression of the already diffused B_z, the B_z field continues to rise near the hardcore, at times around sheath equilibrium, at the

rate of approximately 100 G/μsec. A similar rate of diffusion at earlier times would account for the observed fields. Thus we have the diffusion rate of the external field of 3 kG through the plasma sheath which is 3 cm thick and has an inner radius of 7 cm. Using this in

$$B = B_o \left(1 - \exp \frac{-t}{\tau}\right) \qquad \ldots (1)$$

we obtain $\tau = 30$ μsec. Also $\tau = 2.10^{-13} T^{3/2} r \delta$ and with $r = 10$ cm, $\delta = 3$ cm then $T \sim 3$ eV. This is intermediate between the directly measured value obtained with the double probe and the value obtained from measurements of the electric and magnetic fields.

Azimuthal Field Diffusion

At gas current maximum the B_θ field has the values of 3.4 kG and 1.4 kG at $r = 7$ cm and $r = 10$ cm respectively, i.e. across the sheath thickness. From 10 μsec onwards, although the driving B_z field does not reach its maximum until 15 μsec, the gas current falls at the rate of approximately 3 kA/μsec. If we assume the B_θ field to diffuse through the sheath at the same rate as the B_z then at 11 μsec we might expect the field at $r = 10$ cm to be 1400 + 60 gauss with only a small change at $r = 7$ cm due to the difference in magnetic volumes. This diffusion would correspond to a reduction of axial gas current from 50 kA to 47 kA in the period 10 μsec to 11 μsec. Thus these approximate calculations indicate a degree of consistency between the measured field diffusion and the plasma temperature.

Effect of Pressure on Diffusion

While having a marked effect on the initial breakdown the pressure had little effect on the subsequent diffusion except at pressures below 10 mTorr. At these low pressures marked instability and thickening of the sheath were observed and were probably connected with the breakdown phase.

The effect of pressure on the sheath thickness (δ), and current density (j_z), is given in Table 1 below. The full range of pressures investigated was 8, 15, 30, 40 and 65 mTorr, but as the discharge configuration and parameters showed little

variation for pressures > 30 mTorr the higher pressures are all included under that heading.

Table 1

Effect of Pressure on Sheath

p (mTorr)	⩾ 30			15			8		
t (μsec)	4	8	12	4	8	12	4	8	12
j_z(A/cm²)	260	340	340	220	550	600	190	420	320
δ (cm)		2.4	2.7		1.2	1.6		1.7	2.9
I_z(kA)			62.5			55			50

This table shows the marked reduction in the sheath thickness as the pressure falls below 30 mTorr and the corresponding increase in the axial current density. Fig.10 shows the current densities at 8 μsec and 12 μsec.

For the detailed investigation the 15 mTorr value was chosen as it was the lowest pressure at which reliable breakdown and reproducible operation was ensured.

EFFECT OF B_{zo} FIELD

If the igniters are not used the B_{zo} field has a strong effect on breakdown. The breakdown at 30 mTorr, normally rather poor, is enhanced by reverse B_{zo} and inhibited by forward B_{zo}. When the igniters are used these effects are much reduced but still observed.

With igniters and B_{zo} fields of 500 G or more the discharge behaviour is significantly affected. Figs.11 and 12 show the B_z and rB_θ profiles at current maximum for the three cases of B_{zo} = 0, - 750 G and + 2000 G. Although the magnitude and radial distribution of the axial current densities are similar in all cases the same is not true of the azimuthal component. Without B_{zo} the j_θ profile is well defined and moves from r = 15 cm to its equilibrium position at r = 7 cm in the first 10 - 12 μsec. With 2000 G forward B_{zo} a similar radial distribution is observed but the magnitude is much reduced as would be expected, to give the same inward force in the presence of a higher B_z field. With 750 G of reverse B_{zo} both the radial distribution and magnitude are altered. Azimuthal

current is flowing at all radii less than 9 cm, and from the complete set of field profiles it appears that breakdown takes place at $r = 11 - 12$ cm and not, as is usual, on the wall.

THE DISCHARGE BEHAVIOUR - DETAIL

It was apparent from earlier work[6] that the FAUST 1 discharge was to a large extent reproducible from shot-to-shot and it was decided to make as comprehensive an investigation as possible of a particular set of conditions.

The conditions used were

(a) Igniter supply system 15 kV, 8000 pF; and
8 kV, 8 μF - used only in latter half of the investigation.

(b) B_θ supply charged 2.4 kV.

(c) B_z supply charged 6.0 kV.

(d) Initial filling pressure 15 mTorr of H_2.

These conditions correspond to an initial rod current of 100 kA. This rises to a maximum value of 120 kA, 5 μsec after the B_z is fired. During this 5 μsec period the strap current drops from 100 kA to 65 kA, while the axial gas current rises from zero to 55 kA.

The effect on the plasma of applying a B_{zo} field in either the forward or reverse directions was studied within these conditions; the B_{zo} range being 0 to ± 2 kG.

MAGNETIC FIELD PROFILES

Using a Hall effect probe the radial profiles of the vacuum fields were obtained,

(i) in the radial plane midway between the electrodes, and
(ii) in the radial plane 2 cm below the anode surface.

These profiles are given in Fig.13. The azimuthal field profile at electrode and centre is the same within the errors of measurement and both show the same departure from the theoretical $1/r$ dependence at radii greater than 12 cm. This is primarily due to the use of sixteen straps as return conductors. The axial field

profile at the centre is reasonably uniform in contrast to that near the anode. The B_z flux (which is of too high a frequency to penetrate the electrode) is forced out of the gap between the electrode and the edge of the B_z coil. This produces a high field region in the neighbourhood of this gap and is the reason for the sharp maximum in the vacuum profile at the anode at radius 14 - 15 cm. There is, therefore, a strong radial component of magnetic field near the electrodes.

Using the conditions described above the B_z and rB_θ profiles for the discharge were obtained and are shown in Fig.14. The j_z and j_θ profiles of Fig. 15 were obtained in the usual manner (see below under 'Derived Quantities').

One sees that the plasma develops near the wall, and in the central region moves steadily in to its equilibrium position centred on radius ~ 7 cm. The sheath half-width (i.e. thickness at half-height) remains at ~ 2 cm, from about 6 μsec until late in the half-cycle at ~ 25μsec. At the electrode however the plasma movement is less and the equilibrium radius for the sheath is ~ 12 cm. The half-width is the same as at the centre but the current density is, in general, reduced. The plasma does not actually leave the wall until 6 - 8 μsec at the electrode compared with 2 - 4 μsec at the centre.

The reproducibility of the FAUST 1 discharge is best illustrated by an oscillogram of three superposed shots, as in Fig.16. Each trace is of the B_θ field in the central radial plane, as measured by two diametrically opposite probes of approximately equal sensitivity, and both at $r = 8$ cm (i.e. in the centre of the sheath). It should be noted that the true base-line to which these traces are referred, is the sloping continuation of the initial straight portion of the traces. This slope is due to the slow B_θ pulse on which is superposed the faster discharge pulse. The B_θ traces were far more sensitive than B_z to any form of plasma perturbation, and the greatest degree of irreproducibility observed was as illustrated; that of B_θ traces in the sheath. Excluded here is the case of deliberately induced instability using a trapped B_{zo} field. The degree of fluctuation observed in superposed shots of B_z field was always very small and

and was usually only a thickening of the trace. All fluctuations observed were of low frequency.

THE ELECTRIC FIELDS

The axial and azimuthal fields were measured at the centre and at the anode using a floating or electrostatic probe. The results of these measurements are given in Fig.17. Like the magnetic fields, they were reproducible to a large degree from shot-to-shot, and one noticeable feature was the complete absence of any high frequency fluctuations. The electric fields were closely related to the sheath position and appear to move with the sheath during the compression stage.

It is immediately apparent that, whereas at the centre the magnitude of the azimuthal is greater than the axial field, this situation is reversed at the anode where the axial field is the larger.

Measurements were also made of the sheath potential[7] at both the anode and the cathode. At the anode the potential drop across the 2 cm gap between the probe tip and the electrode surface was measured using a potential divider and oscilloscope, as was the potential between the electrode surface and the tip of an igniter pin, a distance of some 5 cm. The potential drop as given by both these measurements was $\sim$ 150 volts which indicates that most of this potential was developed across the small layer, less than 2 cm thick, in contact with the electrode surface. Any increase in distance from this region only added the small contribution from the general axial field of a few volts/cm. For this reason the potentials measured at the cathode between igniter pin and electrode are taken as being due to the cathode sheath potential. This was found to be $\sim$150 volts also, and both potentials were very similar in temporal variation as well as magnitude. The application of B_{zo} in either forward or reverse direction had little effect on these potentials, only a slight decrease in reproducibility being observed. The level of irreproducibility rose as the amount of applied B_{zo} increased.

THE DOUBLE PROBE MEASUREMENTS

Initial exploratory measurements with a biassed double probe[8] showed the

discharge to be sufficiently reproducible for the shot-to-shot variation in the current through the double probe to be small; as a consequence the determination of particle density and temperature using a double probe was feasible. As an illustration of the degree of variation, Fig.18 shows three sets of three superposed oscillograms of probe current. It is interesting to note that the reproducibility is maintained well into the second half-cycle.

The double probes were sensitive to noise from the B_z spark gaps which is evident at the beginning and end of the half-cycle. The noise level is small throughout the rest of the pulse and did not affect the analysis of the oscillograms. The signal from the double probe will also contain a component due to the electric field in the region. This contribution was always small, less than 2% of the mean, and did not seriously affect the analysis of the double probe oscillograms. Conventional double probe techniques were employed. the bias potential and current supplies were by battery and capacitors respectively, while the whole system was isolated from the recording and measuring circuit by a pulse transformer of 10 Mc/s frequency response.

A complete run of approximately 100 shots was sufficient to cover the bias range $-36\,V$ to $+36\,V$, after the probes had been discharge cleaned with a bias of $120\,V$. The data was analysed at 6, 8, 10, 12, 15 and 21 μsec, and the bias curve corresponding to each time was constructed and the saturation current determined. By generating the logarithmic characteristic of the bias curve the temperature is obtained directly from the slope, and by combining this with the saturation current and the probe area the particle density is calculated. A typical bias curve is given in Fig.19. This process was repeated across the radius of the tube, (measurements being made at the centre and at the electrode), and the results are presented as:

(a) radial particle density profiles at successive times, at the centre (Fig.20) and at the electrode (Fig.21);

(b) radial temperature profiles at successive times, at centre (Fig.22) and at the electrode (Fig.23);

(c) radial kinetic pressure profiles at successive times, at the centre (Fig.24) and at the electrode (Fig.25).

(The derivation of (c) involves the assumption that $T_i \sim T_e$. Since the collisional relaxation time is ~ 1 μsec this assumption is justified.)

The formation, position and motion of the sheath as indicated by the particle density agree well with those given by the derived current density.

The lower limits of measurable density and temperature, determined by the area of the double probe electrodes, were 5×10^{13} cm^{-3} and 0.1 eV. In the central radial plane the particle density and temperature were below these values, both at the wall and at the hardcore (i.e. density at wall of the order of 1% of density in sheath); the discharge channel being well defined and centred on radius ~ 8 cm.

The apparent splitting of the sheath into two portions from 15 μsec is probably due to an error in the value of particle density derived from the run at 8 cm. This measurement was carried out several days previously to those at other radii which were done concurrently, and during this interval, the tube was let up to atmospheric pressure with dry nitrogen as the filling gas. It is not obvious however why the difference should only occur after 15 μsec, the behaviour being normal up to that time. Although the effect cannot be definitely discounted as spurious, no other evidence is forthcoming from other diagnostics to substantiate it.

At the electrode the plasma leaves the wall much later than in the centre and both particle density and kinetic pressure have a relatively large value at the wall until 6 - 8 μsec. The density is again less than 5×10^{13} cm^{-3} at the hardcore throughout the whole pulse.

The maximum values of particle density and electron temperature observed in the centre are 3.5×10^{15} ions-cm^3 and 9.2 eV whereas at the electrode, although the temperature still peaks at 9.2 eV the maximum particle density has dropped to 1.0×10^{15} ions-cm^{-3}. This ratio of $\sim 4 : 1$ between particle densities at centre and electrode is generally true throughout the pulse, whilst there is little difference between the observed temperatures.

The effect of pressure and of trapped B_{zo} (both forward and reverse) were

measured, although not in a complete manner. The time dependence of particle density and temperature at the equilibrium sheath position, at both centre and electrode, were determined at 15 mTorr, and at 30 mTorr. The results of these measurements are given in Fig.26 which indicates that although the temperatures are but little affected the particle densities show a pressure dependence. At the centre at 15 mTorr the particle density rises to a maximum at 12 μsec (10 μsec at the electrode) and then falls for the rest of the half-cycle. With an initial filling pressure of 30 mTorr however the increase in particle density is sustained until 15 μsec (12 μsec at the electrode), and moreover the ensuing decrease is much less marked than in the lower pressure case. The discharge current changes corresponding to these sets of conditions are in the same direction but very much smaller. The gas current increases from 55 kA at 15 mTorr to 62 kA at 30 mTorr, an increase of 12½% compared with the doubling of the particle density.

The effect of initially applied B_{zo} field on the particle density and temperature is given in Fig.27 for the sheath equilibrium position, for both forward and reverse B_{zo}. The difference between the cases when B_{zo} field is applied and when it is absent would seem to be more marked than any differences caused by the direction of the B_{zo} field itself. In general the behaviour up to peak current in all cases is very similar but after this time the effect of B_{zo} becomes more apparent. Although the temperatures at the centre and at the electrode, as well as the particle density at the centre, are little affected, the particle density at the electrode is greatly increased; at least doubled for every case investigated. A possible explanation for this increase is that in this case of applied B_{zo} some of the magnetic flux will be anchored in the electrodes in direct contrast to the usual case when the electrodes have no flux lines penetrating them.

THE DERIVED QUANTITIES

This section describes the results of calculations which use the directly measured quantities given above, to obtain values for β, plasma resistivity, temperature, and pressure. As discussed above, the tube conditions were kept fixed for most of the measurements to give consistency. The effects of variation

of pressure and applied B_{zo} on these parameters were not investigated.

Beta

The ratio of plasma pressure to magnetic pressure $\beta = \frac{8\pi p}{B^2}$ is a useful quantity in assessing the value of pressure balance equations (see below), and effects of instability. It involves the magnetic field, both B_θ and B_z from probe results, and nkT from double probe measurements of n and T, with the assumption that $T_i = T_e$ (see above under 'Double Probe Measurements').

The mean value of B was about 3.3 kG at most times and radii during the discharge, and that of p about 5×10^4 dynes-cm^{-2}. The value of β is given in Table 2 below.

Table 2

Value of β throughout the Pulse

Radius (cm) \ Time (μs)	6	8	10	12	15
6				.079	.13
7		.004	.022	.047	.15
8		.018	.071	.19	.10
9		.091	.16	.17	.12
10	.032	.066	.086	.007	.001

It can be seen that β generally increases with time, and is very small up to 8 μsec. Its peak value follows that of the sheath centre, which is more or less a diagonal line from (6, 10) to (15, 7) on the table.

Pressure Balance

From the difference in the magnetic pressures $(j_z B_\theta - j_\theta B_z)$ the plasma pressure can be deduced[9]. From

$$\text{curl } \underline{B} = 4\pi j$$

we have

$$j_z = \frac{1}{4\pi r} \frac{\partial}{\partial r} (rB_\theta) \qquad \ldots (2)$$

and

$$j_\theta = \frac{1}{4\pi} \frac{\partial}{\partial r} (B_z) \quad . \qquad \ldots (3)$$

The equation for p may be written

$$\frac{\partial p}{\partial r} = \frac{-1}{4\pi} \left[\frac{B_\theta}{r} \left(\frac{\partial}{\partial r} \cdot rB_\theta \right) + B_z \left(\frac{\partial}{\partial r} \cdot B_z \right) \right] \qquad \ldots (4)$$

where the inertial term $\frac{\partial}{\partial t}\left(\rho \frac{dr}{dt} \right)$ has been neglected.

From the measured values of B_θ and B_z, the quantity $\frac{\partial p}{\partial r}$ can be drawn for any time. The pressure p is then obtained by integration. The integration constant means physically that a pressure p must be assumed at some radius in the integration interval, usually at the boundary. In our case, the fact that no gas current flows at radii < 6 cm or > 13 cm encourages the assumption that $p = 0$ both on the hardcore surface at $r = 1.2$ cm and on the outer wall at $r = 15$ cm.

Fig.28 shows the value of $\frac{\partial p}{\partial r}$ at $t = 15$ μsec when the inertial forces will be smallest. The curve will be zero at rod and wall. Integrating the mean curve from $r = 1.2$ cm outwards, gives the plasma pressure as a function of radius, shown in Fig.29 (full-line). The maximum value is at $r = 8$ cm, and is 8×10^4 dyne-cm^{-2}. The pressure outline corresponds well with the j_θ and j_z profiles which have maxima between $r = 7$ cm and $r = 8$ cm (Fig.30). The indicated value of β at $r = 8$ cm is 0.17.

The dotted line in Fig.29 shows the pressure distribution $(n_e + n_i)$ kT as obtained from T_e and n_i given by the Langmuir double probe. The errors on its points are combined from n_i and T_e; there is clearly a very good agreement with the pressure obtained from the magnetic pressure balance method.

A consideration of the errors involved in the latter method leads to the conclusion that such agreement was rather fortuitous. The shaded area of Fig.28 shows the possible variation in the curve using the allowed spread on the points. In view of the accuracy on j and B already quoted, the products jB carried errors between 10% and 30% and the errors in the difference of products were over 100% where the difference was small. The combined uncertainty is shown in each point.

In determining pressure, the shaded area of Fig.28 is outlined by two extreme paths for integration. These give extremely divergent pressure profiles, and only by making the condition that pressure should be zero at the outer wall (r = 15 cm) as well as at the hardcore, could a reasonable spread be placed on the profile. This was done in fact by integrating from both ends of the radius, and taking common areas.

The β-value of t = 15 μsec was greater than 0.1 at all radii. At earlier times, it was generally lower, and it was found that at all other times, up to 12 μsec, the pressure balance method gave unsatisfactory results, although the curves lay within the 'divergent values' quoted above. It can be stated that the assessment of pressure by this method is quite unreliable for $\beta < 0.15$ for anything but the most reproducible plasma and diagnostic conditions.

Resistivity

The resistivity $\eta_{\parallel}$ was derived from measured electric and magnetic fields, using electrostatic and magnetic probes in consecutive experimental runs. This procedure relies on the good reproducibility of plasma conditions in FAUST 1. Taking $E_{\parallel}$ and $J_{\parallel}$ we have

$$\eta_{\parallel} = \frac{E_z B_z + E_\theta B_\theta}{J_z B_z + J_\theta B_\theta} \qquad \ldots (5)$$

The typical values for $\eta_{\parallel}$ in the sheath centre were around 20×10^{-3} ohm-cm. Towards the sheath edges, and outside it, both j and E tend towards zero, and $\eta_{\parallel}$ become indeterminate.

Electron Temperature

Using the Spitzer relation[10]

$$\eta_{\parallel} = \frac{6.53 \times 10^3 \ell n \Omega}{T_e^{3/2}} \text{ ohm-cm} \qquad \ldots (6)$$

the electron temperature can be found. Taking $T_e \sim 5$ eV and $n_i \sim 10^{15}$ cm^{-3}, $\ell n \Omega$ is then about 8. The values obtained for T_e are shown in Fig.31. They may be compared with the directly measured temperatures (dotted lines) obtained as described above. It can be seen that the indirect method gives a mean electron temperature of around 2 eV; the direct method nearer to 6 eV.

The temperature derived from the resistivity is about 3 times less than the double probe value. It would require $\eta_{\parallel}$ to be 5 times less to remove the discrepancy entirely. Such a large error in $\ell n\ \Omega$, E_z, E_θ, J_z or J_θ is unlikely; the probable errors are included in the points of Fig.31, (see below). The interpretation of the double probe results is questionable due to the presence of a magnetic field in the plasma.

Thus we are left with a rather poor agreement in temperature evaluation from the resistivity and from the double probe. The average temperature calculated rather roughly from diffusion measurements gave 3 eV, about midway between the average values of the methods under discussion (5 eV, 1.5 eV).

The errors which are to be assigned to these derived temperatures are consequent upon the errors in the values of electric and magnetic fields used in the calculations. The values of these parameters used were the 'smooth-curve' value taken from the plotted radial profiles and a fixed error of 10% was taken. The current distributions were calculated using these 'smooth-curve' profiles and a fixed angle of $\pm\ 2^{o}$ taken as the error in the slope on which the current density depends. This angular error may perhaps seem a little harsh, but when the magnetic profile is considered in detail it is, in fact, realistic. As all points on these 'smooth-curve' profiles are themselves the mean of three shots each profile is thus the result of perhaps 50 shots, it is therefore not unreasonable to assume that when the above parameters are combined to produce the resistivity and hence electron temperature, their errors have a gaussian distribution. It is on these assumptions therefore that the indicated errors in the derived T_e are obtained.

The errors in the measured value of T_e are rather more nebulous. Each point in the bias curve, which is the mean of at best three shots, will have a corresponding error and thus the bias curve itself can usually be drawn in a variety of ways. This in turn gives rise to variations in the value of saturation probe current and the associated electron temperature. An estimate was made of the likely spread of these values, and the final electron temperature is the mean

of those produced by variations in the bias curves, with an error which combines this degree of variation with the corresponding variations in the saturation probe current.

The Radial Velocity

The radial velocity of the plasma can be determined from

$$V_r = \frac{\underline{E} \wedge \underline{B} - 2\eta_{\parallel}\ \underline{j} \wedge \underline{B}}{B^2} \qquad \ldots (7)$$

assuming $\eta_{\perp} = 2\eta_{\parallel}$. In Table 3 below the calculated values of V_r are given for the times of 4, 8 and 15 μsec, for the resistivity obtained from measured values of E and B, and obtained from the double probe temperature determination. The value indicated by the magnetic field profiles is also given.

Table 3

Calculated Values of Radial Velocity

Rad.	Time	V_r		
		Resistivity from E and B	Resistivity from T_e	Magnetic profile value
7 cm	4 μsec	0.03 × 10^6 cm-sec^{-1}	0.03 × 10^6 cm-sec^{-1}	1.0 × 10^6 cm-sec^{-1}
8		0.03	0.03	
9		0.07	0.07	
10		0.05	0.07	
11		0.06	0.09	
7 cm	8 μsec	-0.02	-0.03	0.5 × 10^6
8		+0.07	0.14	
9		+0.36	0.36	
10		+0.28	0.41	
11		+0.06	0.05	
5 cm	15 μsec	-0.06	-0.06	~ 0
7		+0.05	-0.06	
8		-0.12	-0.08	
9		-0.06	0.14	

In general, better agreement is obtained with the resistivity value derived from the double probe determination of temperature. However since the two values of resistivity obtained from measurements of E and B and from the double probe temperature determinations themselves differ by a factor 5, then the assumption that $\eta_{\perp} = 2\eta_{\parallel}$ is probably unjustified. If this is true the values quoted above for V_r are meaningless.

Particle Line Density

The particle line densities as a function of time calculated by integrating the measured radial density distributions are shown in Fig.32. A distinctive feature of these results is the consistently lower values of line density near the electrode compared with those at the centre.

Energy Balance

A very crude attempt at an energy balance can be made as follows. From the line density measurements we have

$$\frac{dN}{dt} \approx \frac{5 \times 10^{17}}{10^{-5}} = 5 \times 10^{22} \text{ ions/second/cm.}$$

This requires a power input P_1,

$$P_1 = \frac{dN}{dt}\left[(e\, V_i) + 3\, kT_e \right] , \qquad \ldots (8)$$

where $(e\, V_i)$ is the average energy expended to create an ion pair. The power input. P_2 from ohmic heating is

$$P_2 = \int 2\pi r j^2 \eta \; dr .$$

We can choose the resistivity η to correspond either to the electron temperature of 2 eV derived from measurements of $\bar{E}$ and $\bar{B}$, or to the temperature of 6 eV as given by Langmuir probes. Taking $(eV_i) = 30$ electron volts, we obtain,

$$P_1 = 3.0 \times 10^5 \text{ watts/cm} ,$$
$$(P_2)_{2eV} = 15.0 \times 10^5 \text{ watts/cm} ,$$
$$(P_2)_{6eV} = 3 \times 10^5 \text{ watts/cm} .$$

Thus we have a good energy balance if the electron temperature is in fact ~6 eV. If it is 2 eV then it is necessary to invoke some additional mechanism of energy loss.

The time constant for plasma loss to the electrodes is $\tau_1 \simeq L/c_s$ where c_s is the sound speed $\left(= \left(\frac{kT_e}{M} \right)^{\frac{1}{2}} \right)$ and L the inter-electrode distance, is of the order of 40 μsec and too slow to account for the discrepancy. For thermal conduction to the electrodes by the electron gas the time constant τ_2 is,

$$\tau_2 = \left(\frac{L}{\lambda_{ei}} \right)^2 \frac{\lambda_{ei}}{\bar{V}_e} \qquad \ldots (9)$$

where λ_{ei} is the mean free path for electron-ion collisions and $\bar{V}_e$ the mean thermal velocity of the electrons. With $n_e \simeq 10^{15}$/cc and $T_e = 2$ eV, $\tau_2 \simeq 10^{-3}$ seconds, so that this loss is negligible.

Due to the current flow through the system there is a convective loss of electrons at the anode giving a mean power of,

$$P_3 = \frac{I \cdot V_i}{L} = \frac{5 \times 10^4 \cdot 30}{80} \approx 2 \times 10^4 \text{ watts/cm.}$$

i.e. again much too small.

The power going into instabilities may be estimated as,

$$P_4 = \frac{d}{dt}\left(\frac{B_1 B_o}{4\pi}\right)(\pi r^2) \qquad \ldots (10)$$

where B_1 is the magnitude of the fluctuations in the magnetic field. In practice, $B_1 \leqslant \left(\frac{B_o}{10}\right)$, so taking 10 μsec as the time scale and $B_o \simeq 3 \times 10^3$ gauss gives

$$P_4 \leqslant 3 \times 10^5 \text{ watts/cm.}$$

Consider now the possibility of radiation loss due to the presence of impurities in the plasma. With a temperature of only 2 eV common impurities such as oxygen and carbon will not be stripped into their freely-radiating, lithium-like states (C IV, O VI). Thus we would expect the radiated power to be at least one order of magnitude down on the value given by Seaton[11] for the maximum power radiated, since this is derived making the assumption that all impurity ions are in the lithium-like state.

$$P_5 = \frac{\alpha \cdot n^2 \cdot 2 \times 10^{-24} \; e^{-\psi/T_e}}{T_e^{\frac{1}{2}}} (\pi r^2) \text{ watts/cm ,} \qquad \ldots (11)$$

where α is the fractional impurity content, ψ is the excitation potential of the radiating level and T_e is in electron-volts. Substituting $\alpha = 1\%$, $T_e = 2$ eV and $\psi = 10$ eV gives,

$$P_5 = 3 \times 10^4 \text{ watts/cm length.}$$

Thus it seems unlikely that impurity radiation can contribute seriously to the energy loss when the electron temperature is so low.

Hence we are forced to the conclusion that if the electron temperature is in

fact only 2 eV then energy must be lost from the plasma by some process other than these considered above.

THE STABILITY OF THE DISCHARGE

The stability of the discharge is judged in the usual way, by the degree of reproducibility from shot to shot of various measured parameters, (e.g. $\bar{B}$, $\frac{\partial \bar{B}}{\partial t}$, $\bar{E}$, n, etc.). Since these quantities vary considerably in this respect the method is somewhat imprecise. Sets of superposed oscillograms of B_θ and n at the sheath position have been given in Figs.16 and 18. Figs.33 and 34 shows similar results for $\bar{E}$ and $\frac{\partial B_\theta}{\partial t}$. The fluctuations generally occurred in the period $6 \rightarrow 14$ μsec and the discharge was quiescent before and after that period. The maximum amplitude was ~10% of the mean level. The fastest fluctuations observed were in $\frac{\partial B_\theta}{\partial t}$; the frequencies in this case were $\leqslant 750$ kc/s. Fluctuations in the other parameters generally contained frequencies $\leqslant 200$ kc/s.

The effect of initial gas pressure on the reproducibility was small in the range 15 - 70 mTorr. Below 15 mTorr the gas breakdown became erratic so that 'instability' analysis of this kind was not possible.

THE B_{zo} INDUCED INSTABILITY

The most marked effect on reproducibility was caused by applied B_{zo} (in both forward and reverse directions) which brought about a detectable decrease in stability. The effect was largest with reverse B_{zo}. Figs.33 and 34 show the influence of B_{zo} on the electric field and $\frac{\partial B_\theta}{\partial t}$ signals.

An examination of the time of onset of irreproducibility at each radius shows that the earliest instability occurs at a large radius, closely followed by the inner radii, corresponding roughly to the motion of the sheath.

Since there are both theoretical[1] and experimental[12] grounds for expecting an $m = 0$ tearing-mode (resistive) instability in the reverse B_{zo} case, a correlation analysis was carried out on the $\frac{dB_z}{dt}$ signals from probes on opposite sides of the plasma column. The resultant values of the correlation coefficient R are

given in Table 4.

Table 4

Value of Correlation Coefficient R

Time (μsec)	B_{zo}	
	- 200 G	- 500 G
8	0.42	0.36
10	0.53	0.11
12	- 0.15	- 0.30
14	- 0.06	- 0.27

The three values indicated are the only significant ones (as determined by the Students t test). Since these are positive and substantially greater than zero they indicate the presence of a large $m = 0$ component in the instability.

STABILITY THEORY

Since $j_z B_\theta > 0$ at all radii in the FAUST 1 discharge it should be stable according to infinite-conductivity, magnetohydrodynamic theory[13]. Thus any instabilities must either be due to finite conductivity or to the so-called micro-instabilities which arise from a kinetic treatment of plasma stability taking into account the details of the particle velocity distribution function.

We examine the first (resistive) class of instabilities making use of the extensive theory developed by Furth, Killeen and Rosenbluth[1] for the case of sheared magnetic field.

The mode with the largest wavelength (and therefore the more readily detected), which they find is the tearing mode, or the break-up of the plasma column into several separate pinches. If δ is the thickness of the annular plasma sheath and r its radius, then the mode is only unstable for wave numbers k such that

$$k\,\delta \ll 1 . \qquad \ldots (12)$$

Since the mode is centred on the field spiral we have the additional condition that,

$$k_z B_z + \frac{mB_\theta}{r} = 0 \ , \qquad \ldots (13)$$

and since $k = \left(k_z^2 + \frac{m^2}{r^2} \right)^{\frac{1}{2}}$ the final result is:

$$\frac{m\delta}{r} \left[\frac{B_\theta^2 + B_z^2}{B_z^2} \right]^{\frac{1}{2}} \leqslant 1 \ . \qquad \ldots (14)$$

Thus for the lowest possible mode $m = 1$, and assuming $\delta/r \ll 1$, we get the stability condition,

$$\frac{B_\theta}{B_z} > \frac{r}{\delta} \ . \qquad \ldots (15)$$

In FAUST 1 with $B_{zo} = 0$, $r/\delta \simeq 3.0$ and the condition is satisfied except near the outer edge of the plasma sheath. With increasing forward B_{zo} the stability criterion is violated over an increasing fraction of sheath width and this is consistent with the observed decrease in stability. With reversed B_{zo} there is a null in B_z at some radius and an $m = 0$ tearing mode centred on this radius is then possible. The criterion given above is clearly not applicable in this case. Application of the Bennett relation to the formation of separate 'curtain ring' pinches gives, for the criterion for instability,

$$k_z \delta < \frac{B_z^2}{B_\theta^2} \ , \qquad \ldots (16)$$

where B_z is the magnitude of B_z at the edge of the sheath thickness δ centred on the point at which $B_z = 0$, and B_θ is the value at this null point. In the present experiments the null point occurs well inside the main sheath radius (see Fig.11) and application of this criterion is rather rough, however the ratio of (B_z/B_θ) is $\sim \frac{1}{2}$ so that taking $\delta \simeq 2$ cms, $\lambda_z \simeq 50$ cms. Thus it seems somewhat marginal as to whether these $m = 0$ instabilities can be accommodated within the tube length (80 cms) - in particular the break-up, if it occurs, must be into only a small number (~ 2) of 'curtain rings'.

Experimentally we have only two observations:

(i) the creation of a null in B_z does make the system <u>more</u> unstable;

(ii) these instabilities have a substantial $m = 0$ component. There is no experimental evidence concerning the axial wavelength of these instabilities.

Turning now to the shorter wavelength resistive instabilities, the so-called 'ripple' and 'G'-modes. The e-folding time for these are given by:

$$\tau_{ripple} \sim \alpha^{-2/5} \left[\tau_H^{2/5} \tau_R^{3/5} \right] \qquad \ldots (17)$$

$$\tau_{G\text{-mode}} \sim \alpha^{2/3} \left[\tau_R^{1/3} \tau_H^{2/3} \right] G^{-2/3} \qquad \ldots (18)$$

where $\alpha = k\delta$, $\tau_H = \frac{\delta}{V_A}$, $\tau_R = 4\pi\sigma\delta^2$,

$$G = \left[\frac{g \cdot h}{V_A^2} \right], \quad V_A^2 = \frac{B^2}{4\pi n M} . \qquad \ldots (19)$$

The term g here represents the effective plasma acceleration and may either be due to an actual acceleration of the current sheath $\left(\frac{d^2r}{dt^2}\right)$, or the combination of plasma pressure and field curvature, $g = \frac{p}{nMR} = \frac{c_s^2}{R}$ where R is the radius of the curvature of the field lines,

$$R \approx r \left[\frac{B_\theta^2}{B_\theta^2 + B_z^2} \right]^{1/2} . \qquad \ldots (20)$$

In the present experiments we get the radial acceleration to order of magnitude by dividing the plasma radius by the square of the current rise time to give

$$g_1 = \frac{d^2r}{dt^2} \approx 10^{11} \text{ cm/sec}^2 ,$$

while for a plasma temperature ~ 3 eV, $c_s \approx 2 \cdot 10^6$ cms/sec, and with $B_\theta \approx 3 B_z$,

$$g_2 = \frac{c_s^2}{R} = \frac{5 \times 10^{12}}{10} = 5 \times 10^{11} \text{ cms/sec}^2 .$$

Thus within the accuracy of these calculations the two effects are of similar order. Putting in the experimental parameters with $T_e \approx 5$ eV (since the result is only weakly dependent on T_e we take a mean value of the two determinations) we find the e-folding times for wavelengths in the range 1 - 10 cms are

$$\tau_{ripple} \approx 1 \ \mu\text{sec} ,$$

$$\tau_{G\text{-mode}} \approx 10 \ \mu\text{sec} .$$

Hence the G-mode is not a serious instability in this discharge since it grows too slowly.

If the electron temperature in the discharge is only ~ 2 eV then, as discussed

earlier, the energy containment time

$$\tau_\varepsilon \simeq \frac{3\,n\,kT}{j^2\eta} \simeq 1\ \mu\text{sec}\ .$$

This means that the temperature at any point will be controlled primarily by the balance between joule heating and the large (and unknown) energy loss mechanism. Thus variations of plasma temperature (and hence electrical conductivity) will not be convected or carried along by plasma motions. In this way the ripple mode will be stabilised.

If the temperature is ~6 eV then thermal conduction along the field lines will reduce the growth rate of the ripple mode to some extent[1] but not by an order of magnitude.

Thus we conclude that if the electron temperature is ~6 eV it should be subject to rather mild ripple mode instabilities while if $T_e \sim 2$ eV it should be stable.

ION-WAVE INSTABILITIES

It is well-known from the kinetic theory of plasmas that if the electron drift velocity in the plasma exceeds the sound speed then growing ion-waves should occur[14]. The macroscopic effect of this would be increased resistivity and diffusion rate.

Table 5 gives the measured value of the ratio (V_D/c_s) as a function of time and radius.

Table 5

Ratio of V_D/c_s

Radius (cm) \ Time (μsec)	6	8	10	12	15
6	-	-	-	1.7	0.89
7	-	3.4	1.7	1.4	0.81
8	-	3.4	2.5	0.07	0.60
9	-	1.4	0.17	0.11	0.15
10	3.1	0.49	0.71	0.67	2.3
12	-	-	-	-	4.4

The electron temperature as measured by the Langmuir probe has been used in these calculations. The stable region where $V_D/c_s < 1$ is shown shaded. The main point which emerges is that the centre of the sheath, where the plasma density and the current density are highest, is in the stable region for most of the time.

CONCLUSIONS

(i) The FAUST 1 apparatus produces an extremely stable plasma column with a density $\sim 10^{15}$ electrons/cc and an electron temperature of the order of 5 eV.

(ii) Qualitative agreement with resistive instability theory is obtained in that the addition of an initial B_{zo} either in the forward or reverse direction tends to destabilise the system.

(iii) In the light of present theories the most likely cause of the small residual fluctuations is the 'ripple' resistive instability.

(iv) As a result of the plasma reproducibility it was possible to measure $\bar{E}$, $\bar{B}$, $\bar{j}$, T_e and n, to derive η and β and to test the results for self-consistency. The measurements all indicate a plasma sheath with a width at half-height of 1.5 cms well confined away from the walls and the hardcore. The value of β in the centre is ~ 0.15. The plasma density at the wall is $< 1\%$ of that in the centre of the sheath. A factor of 3 difference is found between the electron temperature deduced from the resistivity ($\sim$ 2 eV) and that measured with a Langmuir double probe ($\sim$ 6 eV).

(v) If the former figure is accepted then it is necessary to invoke some additional and unknown loss mechanism to give an energy balance in the discharge. With the higher figure the power input matches the power consumed in ionizing the gas.

ACKNOWLEDGEMENTS

The authors are grateful to J.G. Griffiths, J. Lunn*, P.A. Mathew, C.F. Parker, A.R. Thomas and A.G. Wardle for assistance with some of the experimental work: to J. Allen and R.A. Burden for the electrical and mechanical maintenance of the apparatus: and to P.A. Worsnop, T.E. James, J.A. Booth, S. Mathews, K. Harries and R. Hunt for the design and construction of the experimental apparatus.

---

* On vacation attachment from University of Liverpool

REFERENCES

1. FURTH, H.P., KILLEEN, J. and ROSENBLUTH, M.N. Finite-resistivity instabilities of a sheet pinch. Phys. Fluids, vol.6, no.4, pp.459 - 484, April, 1963.

2. REBUT, P.H. Instabilités non-magnétohydrodynamiques dans les plasmas a densité de courant élevé. J. Nucl. Energy, Pt C, vol.4, no.3, pp.159 - 168, June, 1962.

3. BICKERTON, R.J. and SPALDING, I.J. The hydromagnetic stability of the hard-core pinch with small electrical conductivity. J. Nuclear Energy, Pt C, vol.4, no.3, pp.151 - 158, June, 1962.

4. BERKOWITZ, J., GRAD, H. and RUBIN, H. Magnetohydrodynamic stability. 2nd International Conference on the Peaceful Uses of Atomic Energy, Geneva, 1958. Proceedings, vol.31, pp.177 - 189.

5. HOPKINS, K.J. Culham Laboratory. To be published.

6. AITKEN, K.L., et al. The stability of linear pinch and hardcore discharges. J. Nucl. Energy, Pt C, vol.6, no.1, pp.39 - 69, January/February, 1964.

7. HARTMAN, C.W. Electrode sheath effects in pulsed, high current discharges. UCRL - 7357, June, 1963.

8. JOHNSON, E.O. and MALTER, L. A floating double probe method for measurements in gas discharges. Phys. Rev., vol.80, no.1, pp.58 - 68, October 1st, 1950.

9. GLASSTONE, S. and LOVBERG, R.H. Controlled thermonuclear reactions. Princeton, Van Nostrand, 1960.

10. SPITZER, L. Physics of fully ionized gases. 2nd ed. New York, Interscience. 1962.

11. SEATON, M.J. The theory of excitation and ionization by electron impact. In Atomic and molecular processes (D.R. Bates, ed.) New York, Academic Press, 1962.

12. BODIN, H.A.B. Observations of resistive instabilities in a theta pinch. Nucl. Fusion, vol.3, no.3, pp.215 - 217, September, 1963.

13. LAING, E.W. Stable configurations of a cylindrical gas discharge. A.E.R.E. - T/M 161, London, H.M.S.O., 1958.

14. STRINGER, T.E. Low-frequency waves in an unbounded plasma. J. Nucl. Energy Pt C, vol.5, no.2, pp.89 - 107, March/April, 1963.

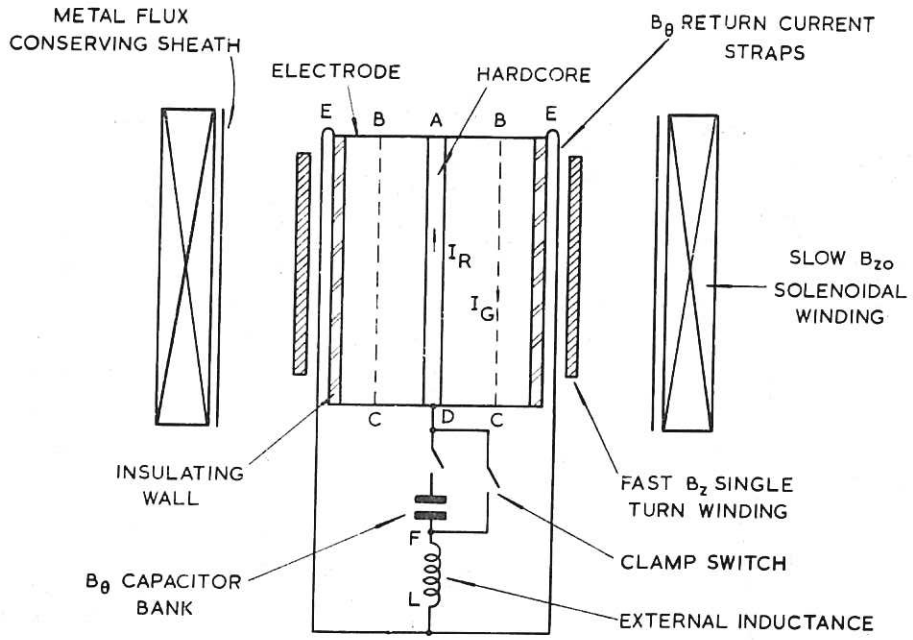

Fig. 1 (CLM-P71)
Schematic arrangement of FAUST 1

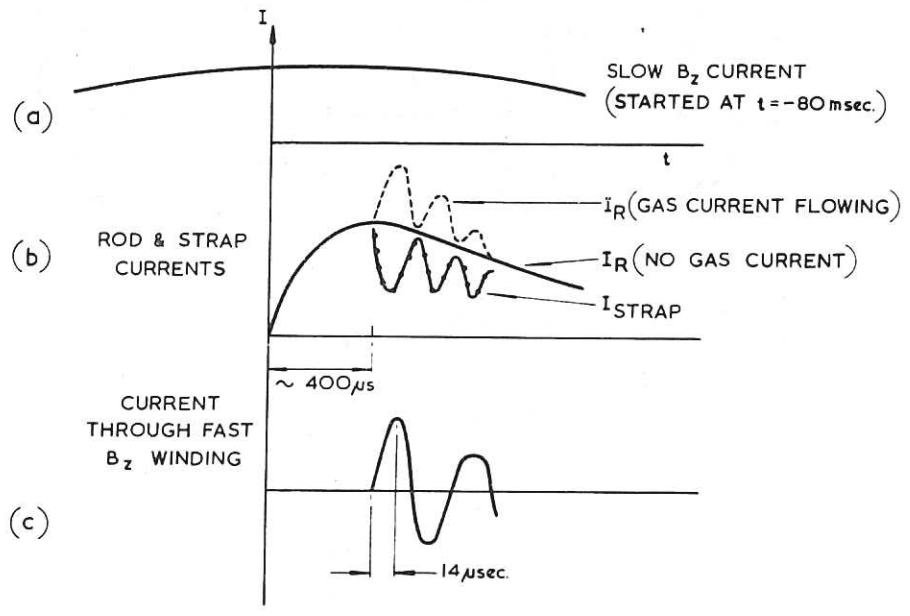

Fig. 2 (CLM-P71)
Currents in various circuits (not to scale)

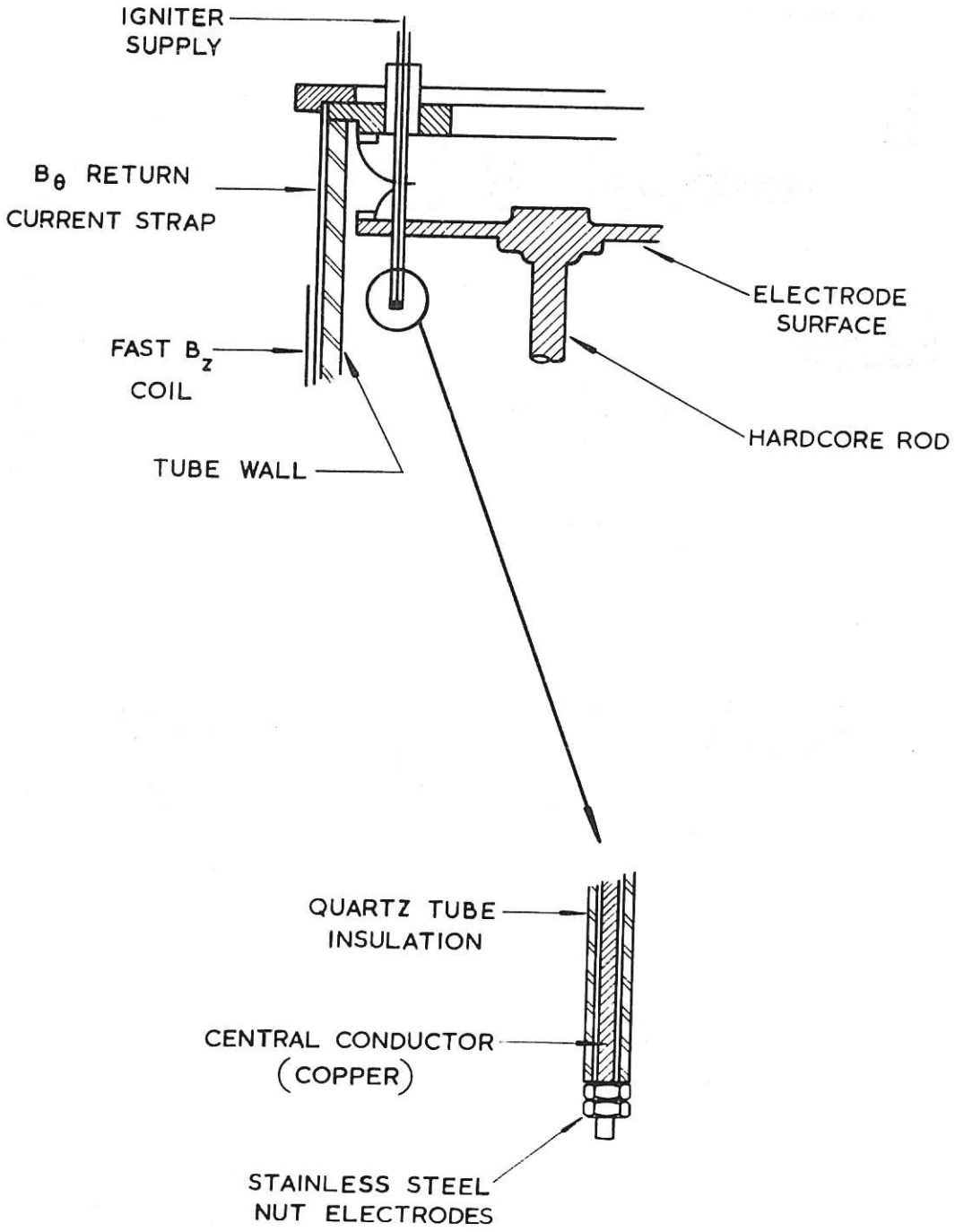

Fig. 5 FAUST 1 igniter pins (schematic) (CLM-P71)

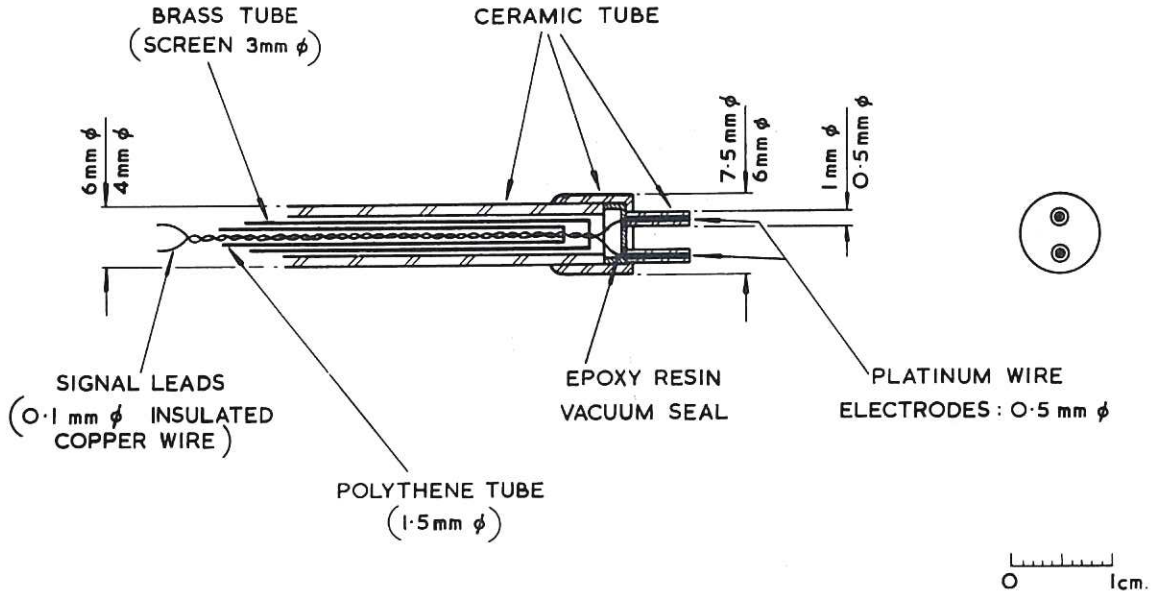

Fig. 6 Double probe construction (CLM-P71)

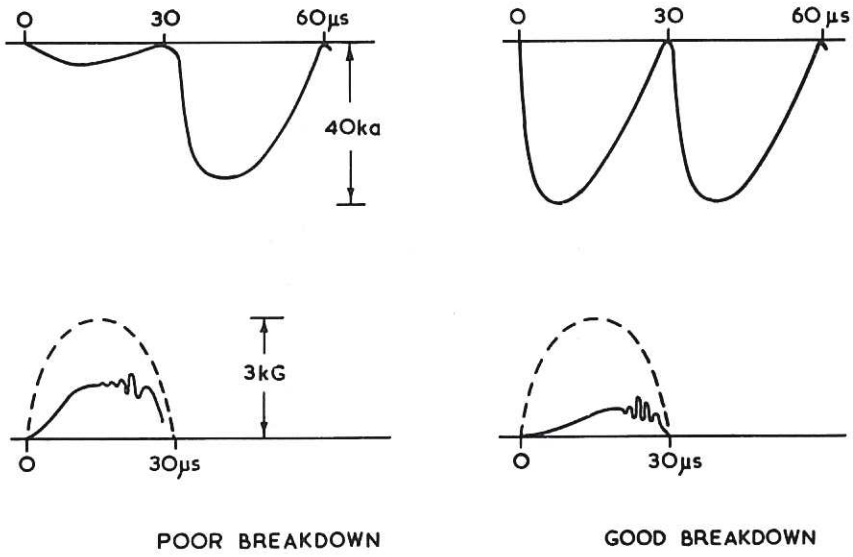

Fig. 7 Degree of breakdown (CLM-P71)

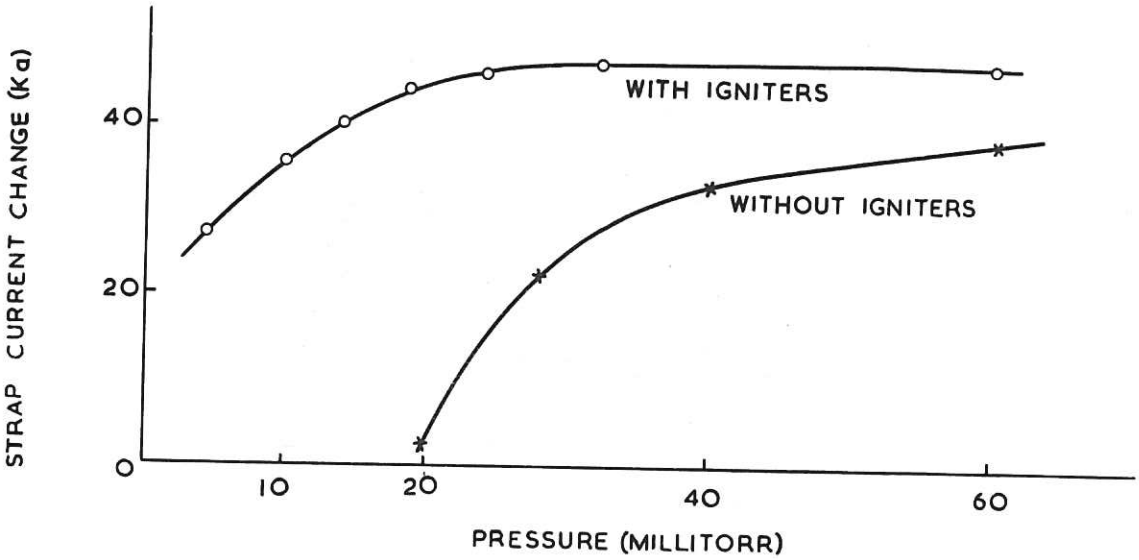

Fig. 8 Effect of igniters (CLM-P 71)

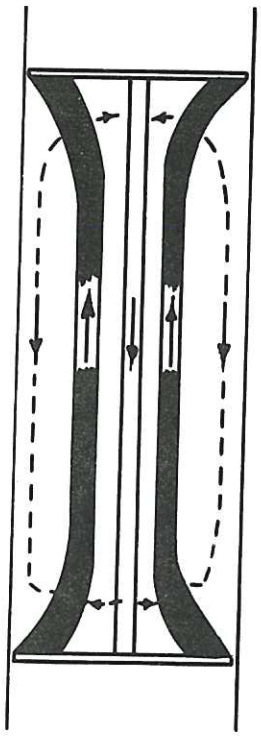

Fig. 9 Possible circulating currents (CLM-P 71)

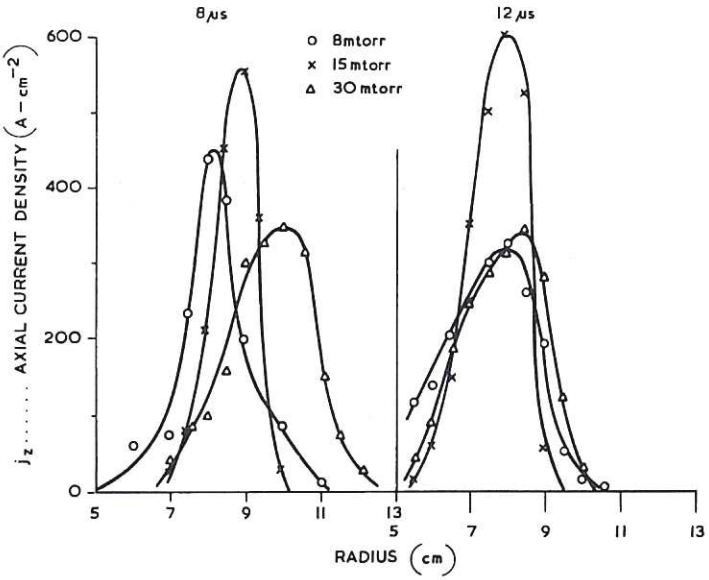

Fig. 10 (CLM-P71)
Effect of pressure on current density profiles

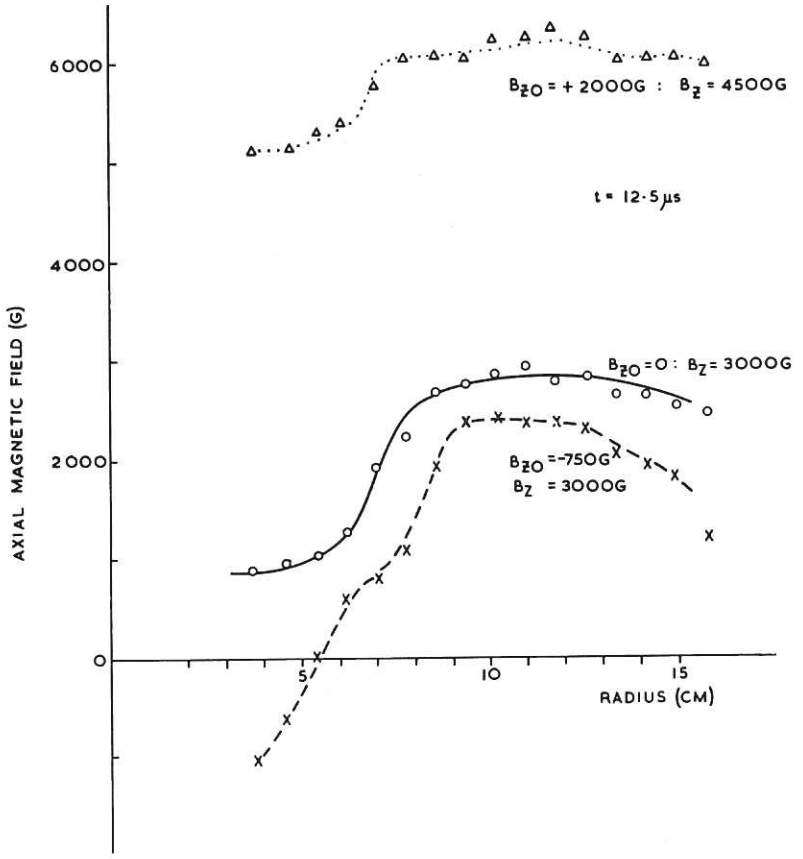

Fig. 11 (CLM-P71)
Effect of B_{zo} on radial profiles of magnetic field at current maximum

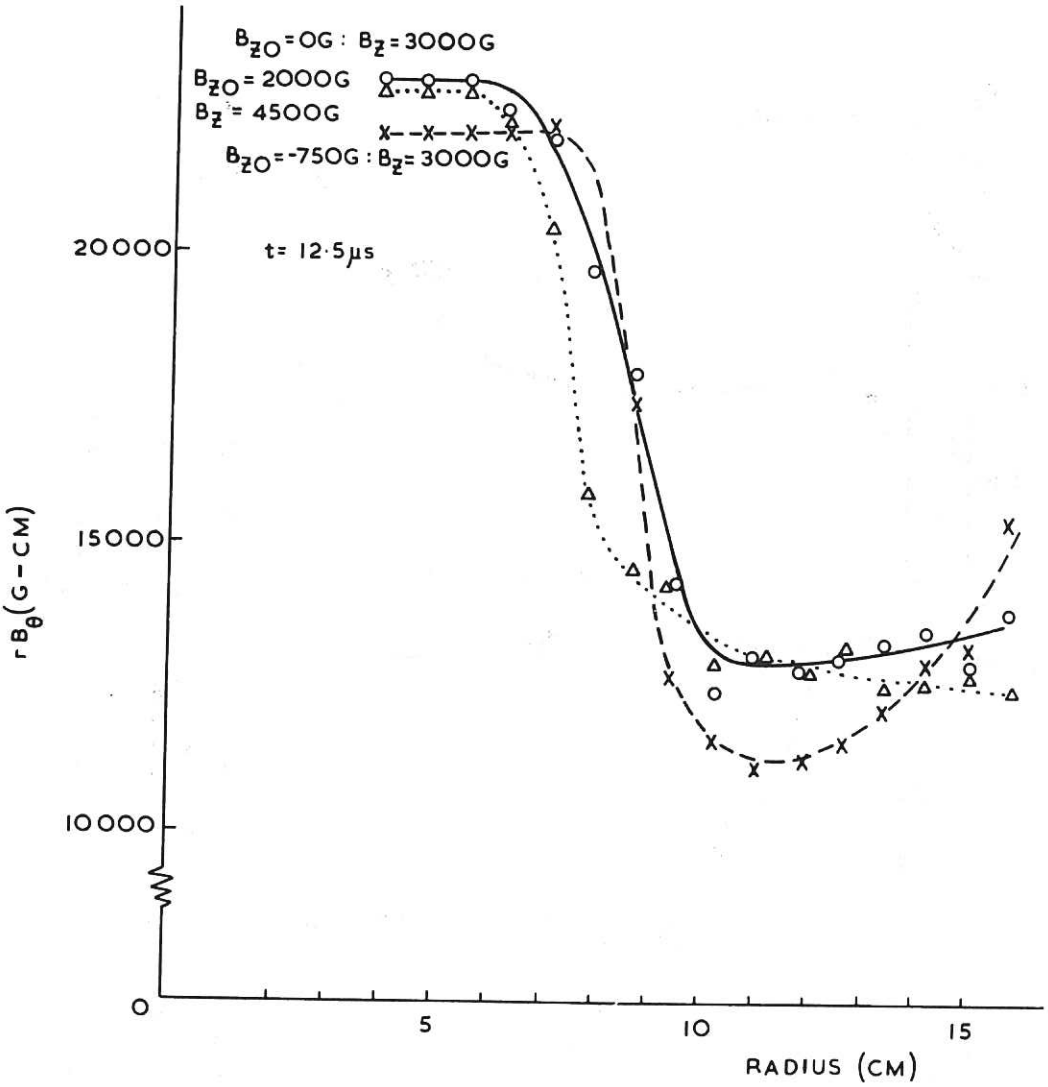

Fig. 12 (CLM-P71)
Effect of B_{zo} on radial profiles of magnetic field at current maximum

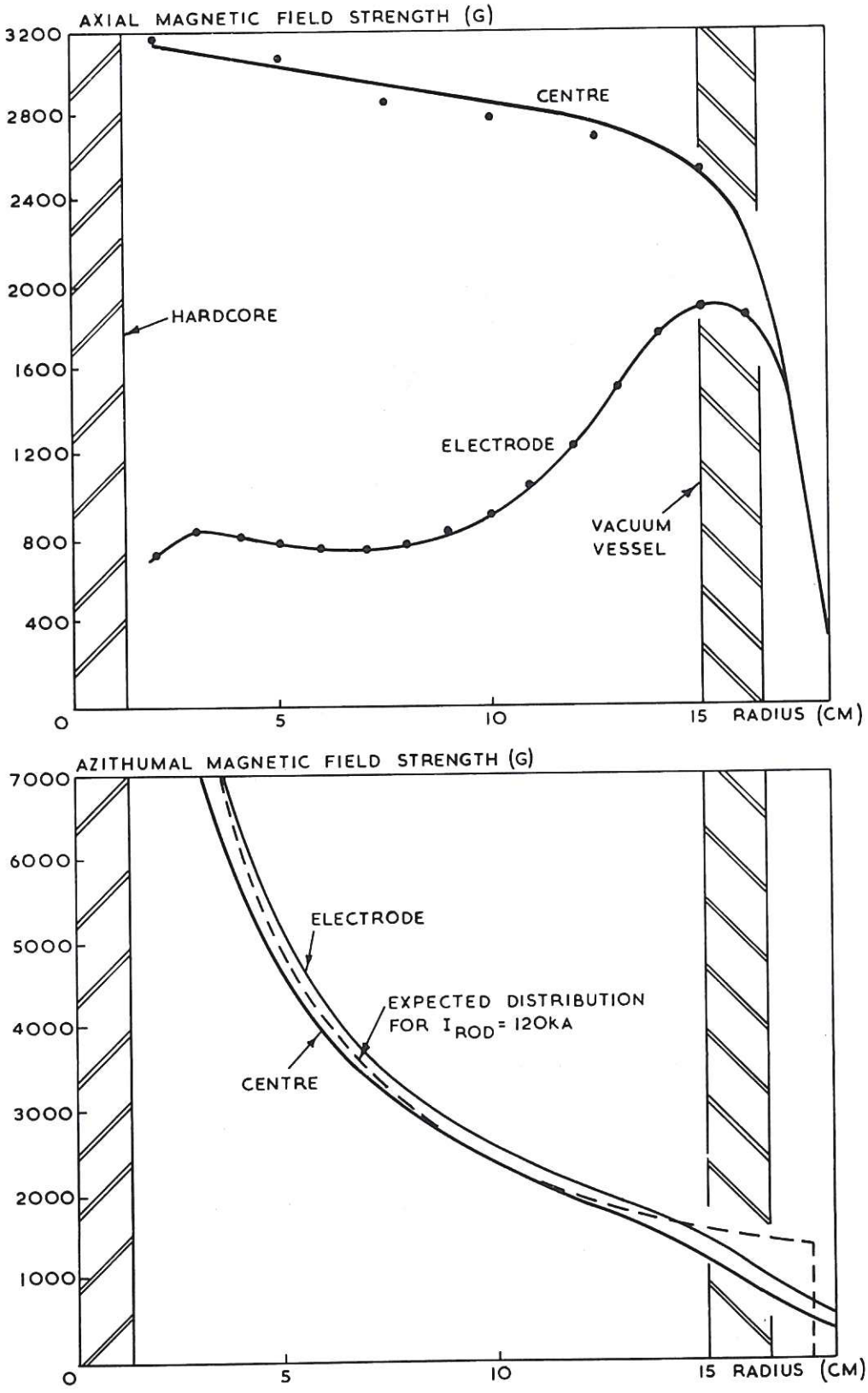

Fig. 13 Vacuum B_z and B_θ fields (CLM-P71)

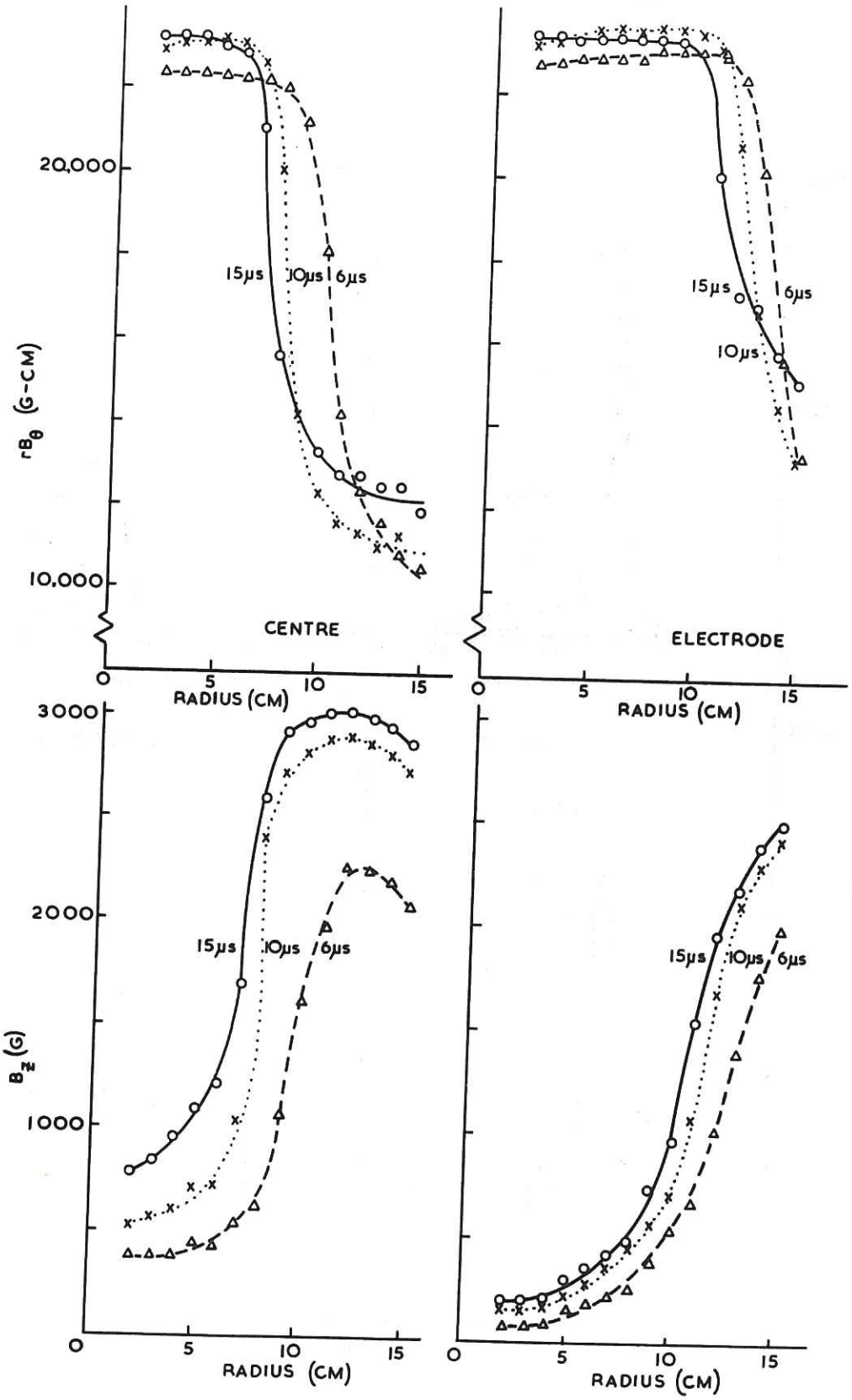

Fig. 14 Discharge profiles of rB_θ and B_z (CLM-P71)

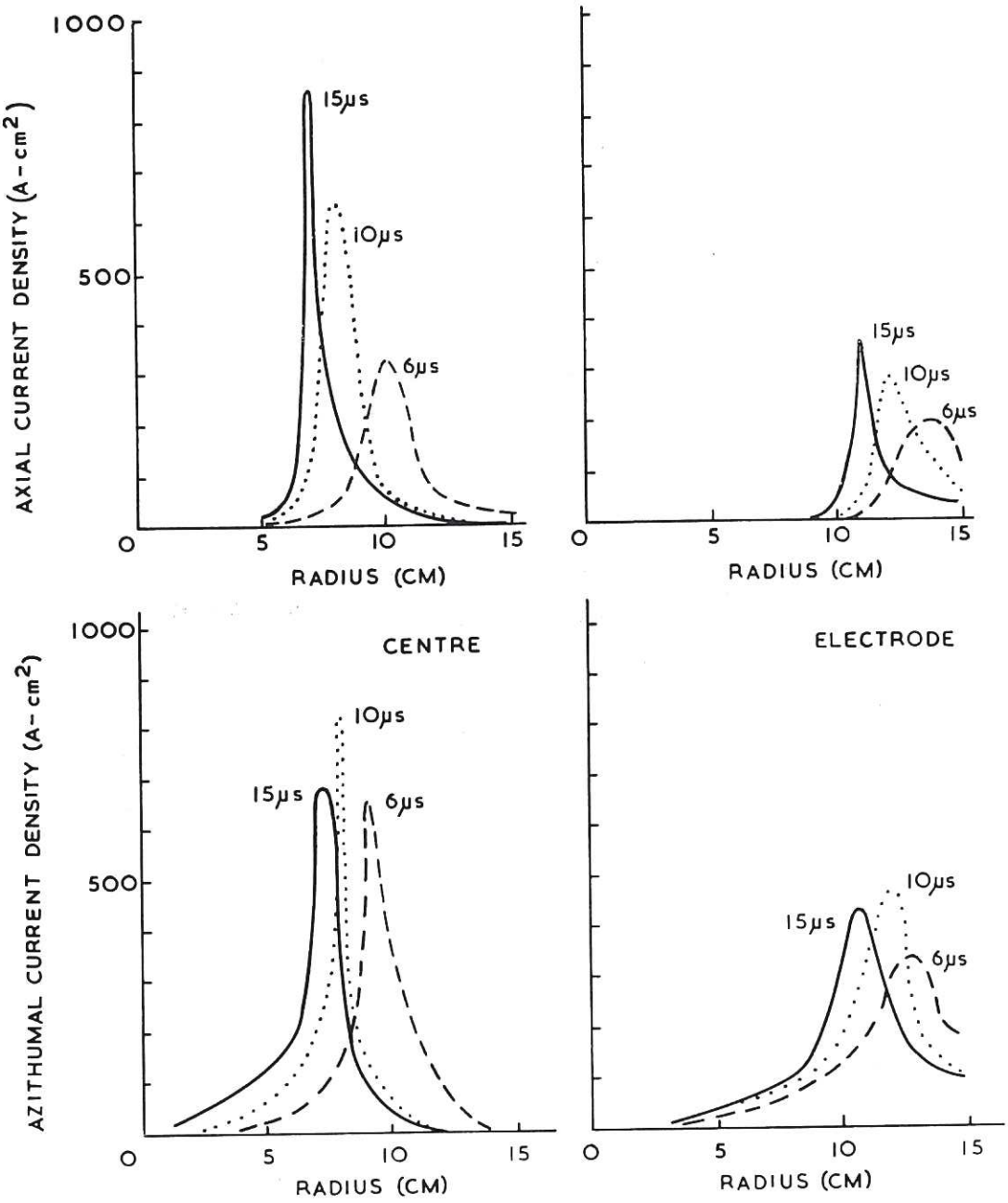

Fig. 15 Current density distributions (CLM-P71)

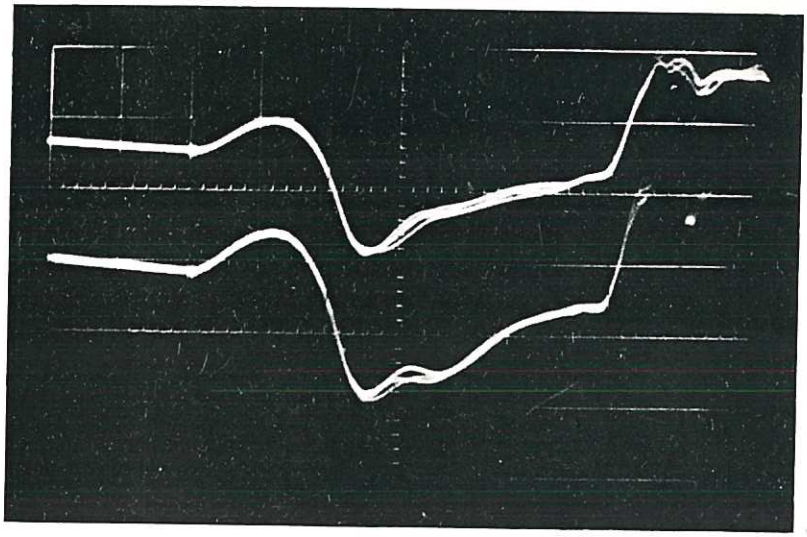

Fig. 16 B_θ overlays (CLM-P71)

Two probes, azimuthal separation 180°, at radius 7 cm
the sheath equilibrium position oscilloscope sweep 5 μs / cm

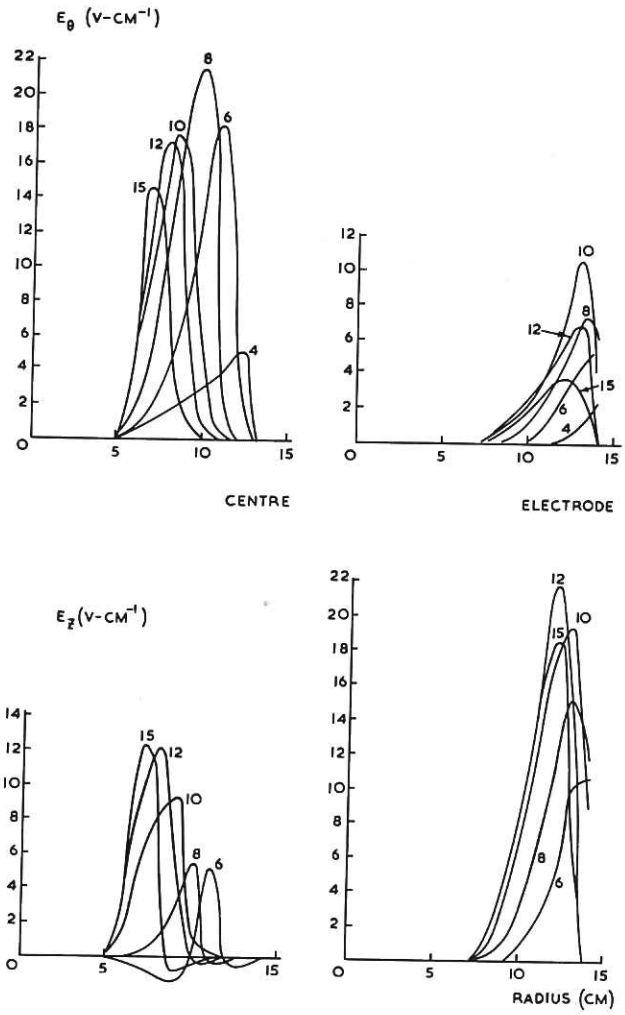

Fig. 17 (CLM-P71)

Radial distribution of axial and azimuthal electric field components

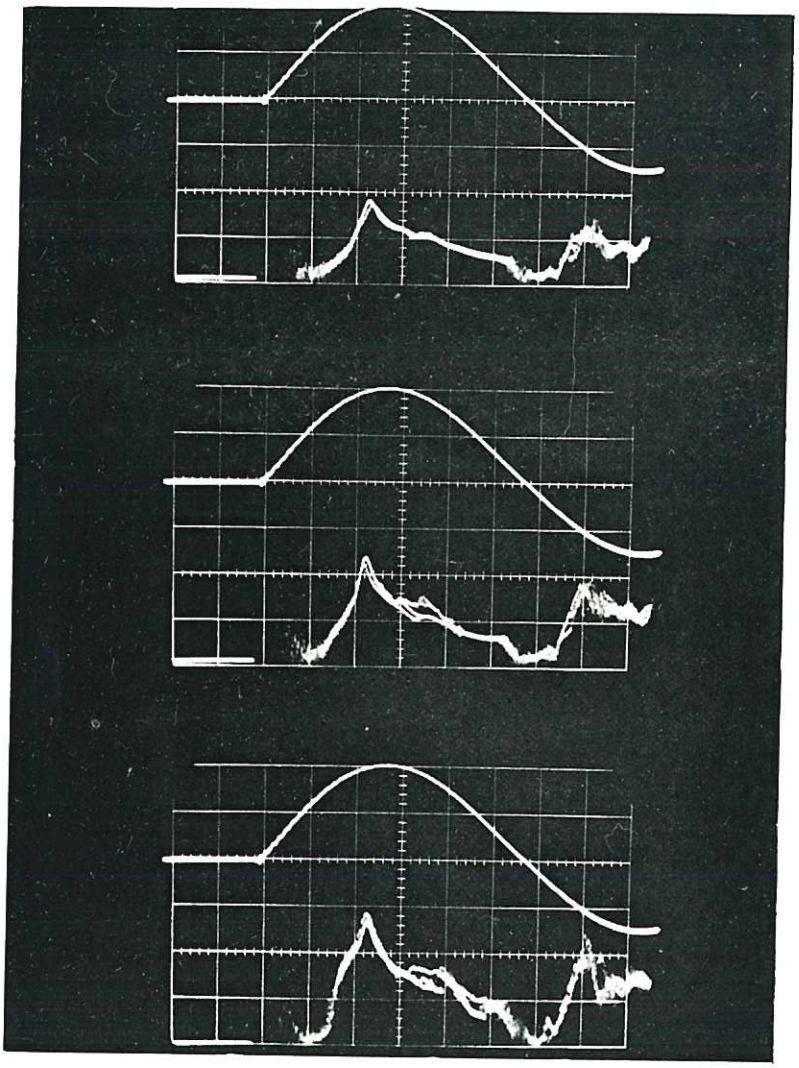

Double probe bias 18 V

Double probe bias 24 V

Double probe bias 30 V

Fig. 18 Double probe reproducibility (CLM-P71)

Upper Trace - B_z Field waveform
Lower Trace - Double probe current
Oscilloscope sweep 5 μs/cm
3 shots per frame
Probe radius 7 cm

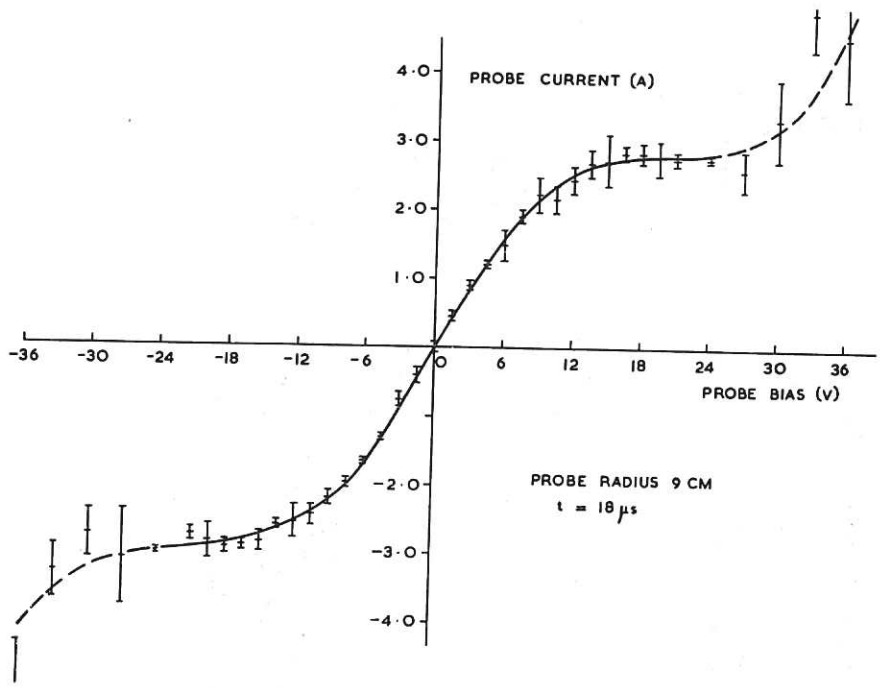

Fig. 19 Double probe bias curve (CLM-P71)

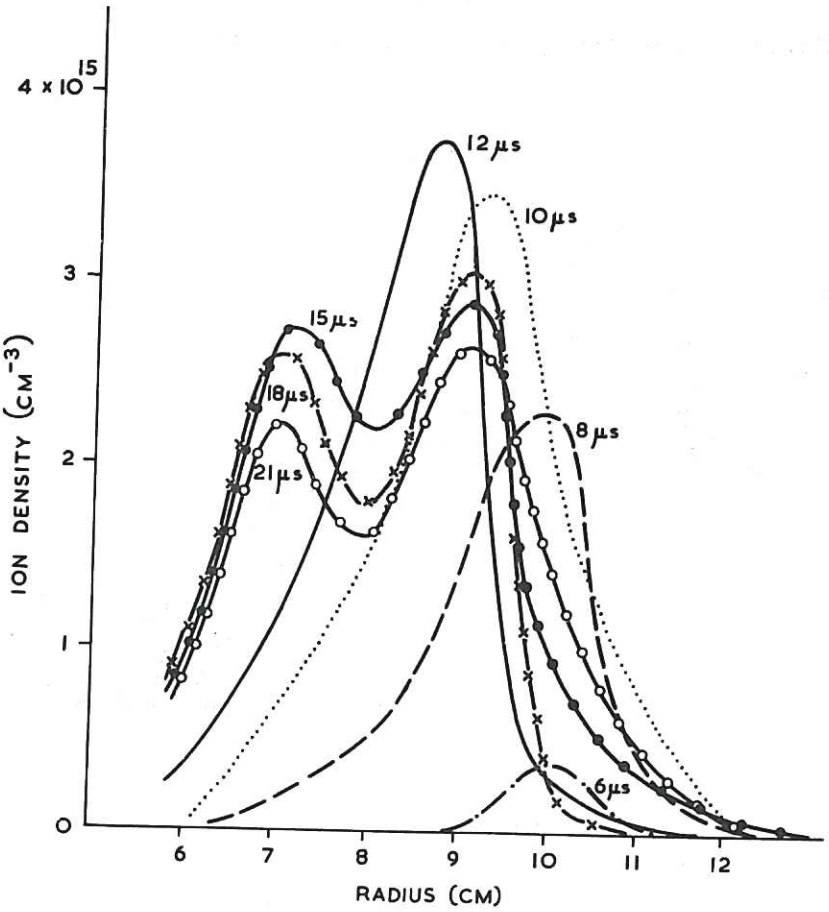

Fig. 20 Radial density profiles - centre (CLM-P71)

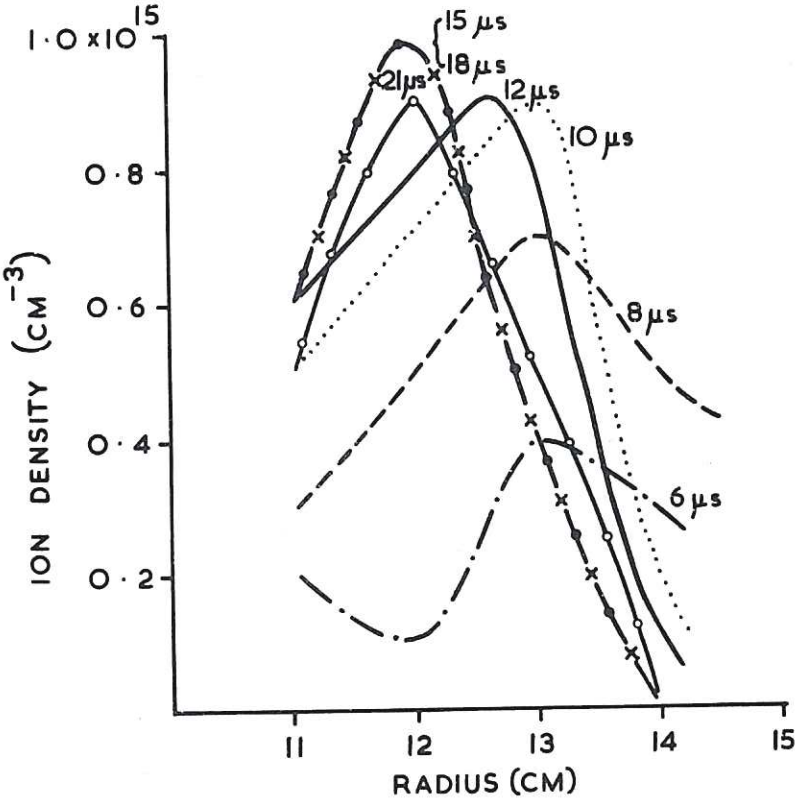

Fig. 21 Radial density profiles - electrode (CLM-P71)

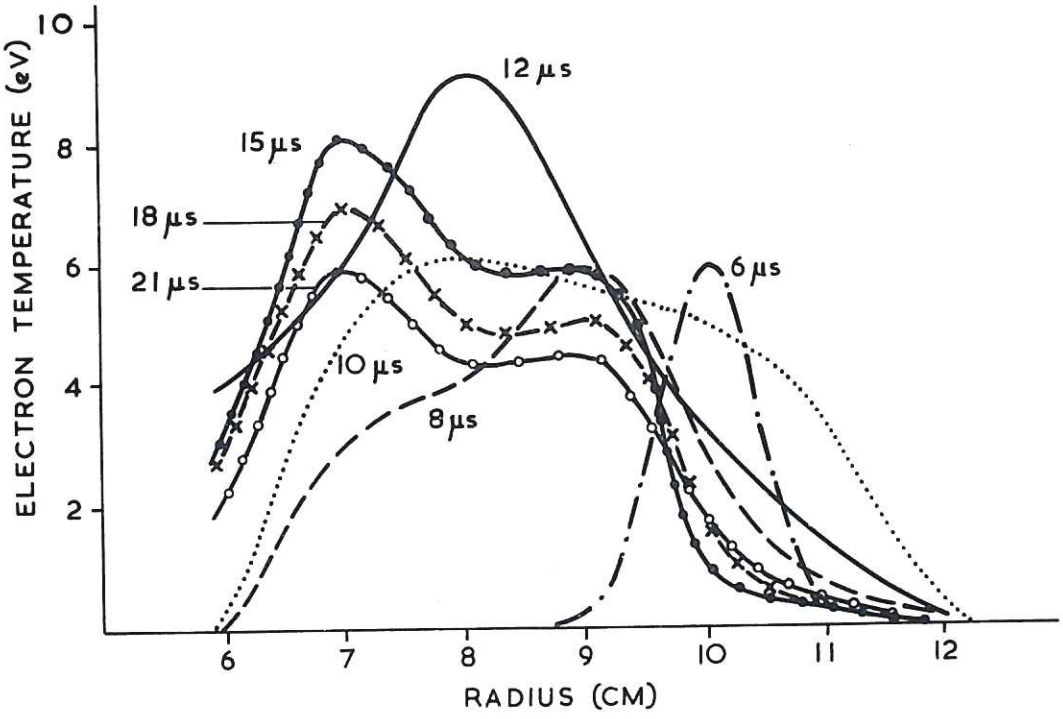

Fig. 22 Radial temperature profiles - centre (CLM-P71)

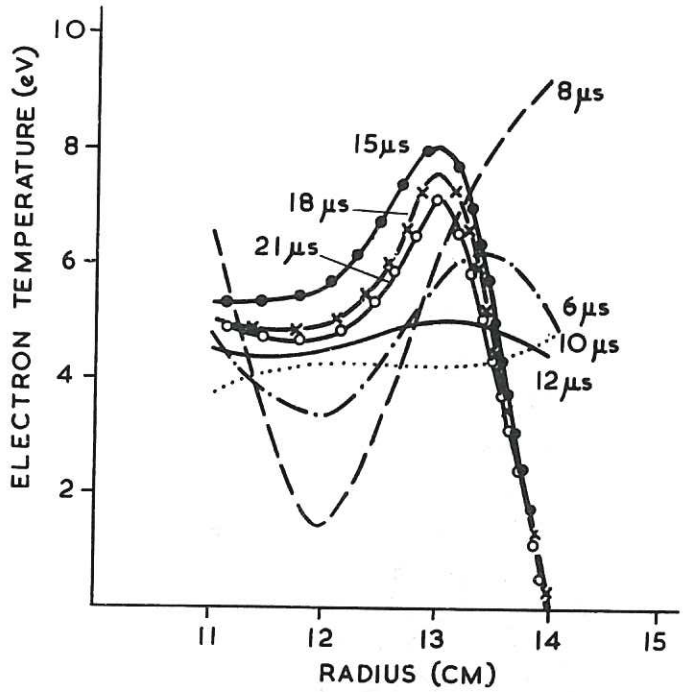

Fig. 23 Radial temperature profiles - electrode (CLM-P71)

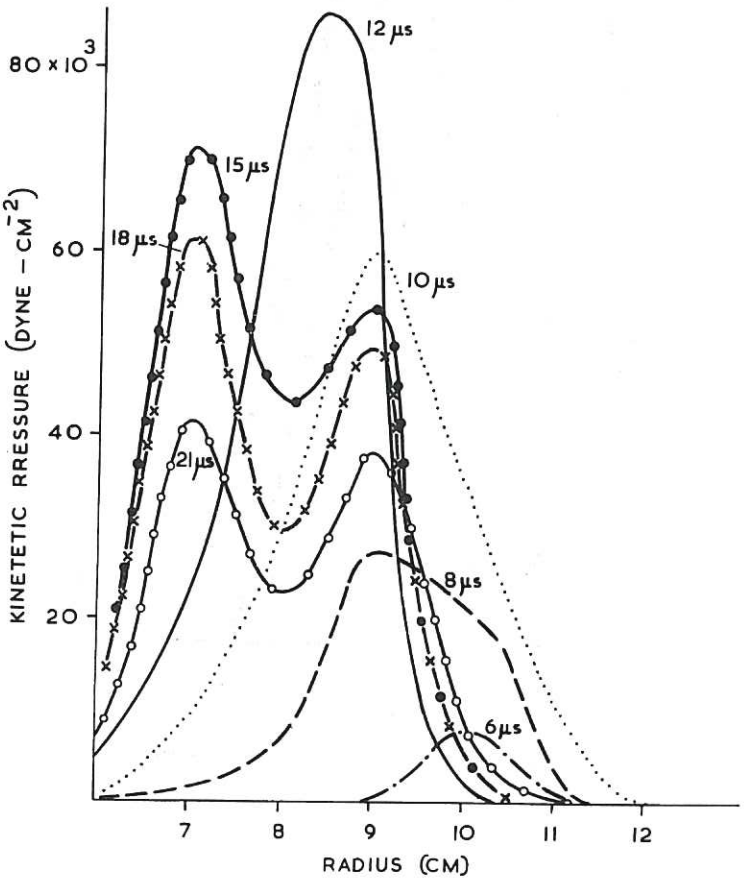

Fig. 24 Radial kinetic pressure profiles - centre (CLM-P71)

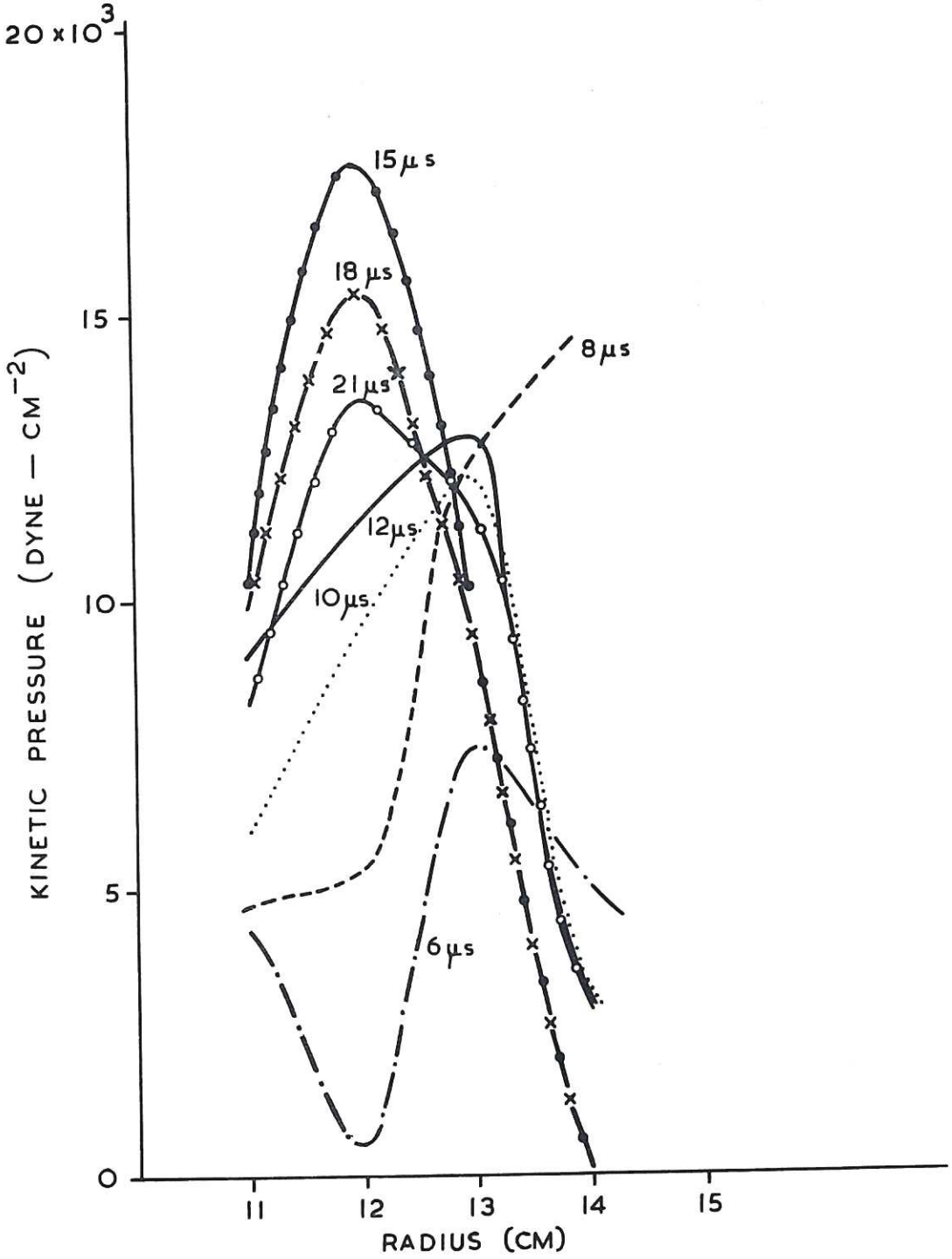

Fig. 25 Radial kinetic pressure profiles - electrode (CLM-P71)

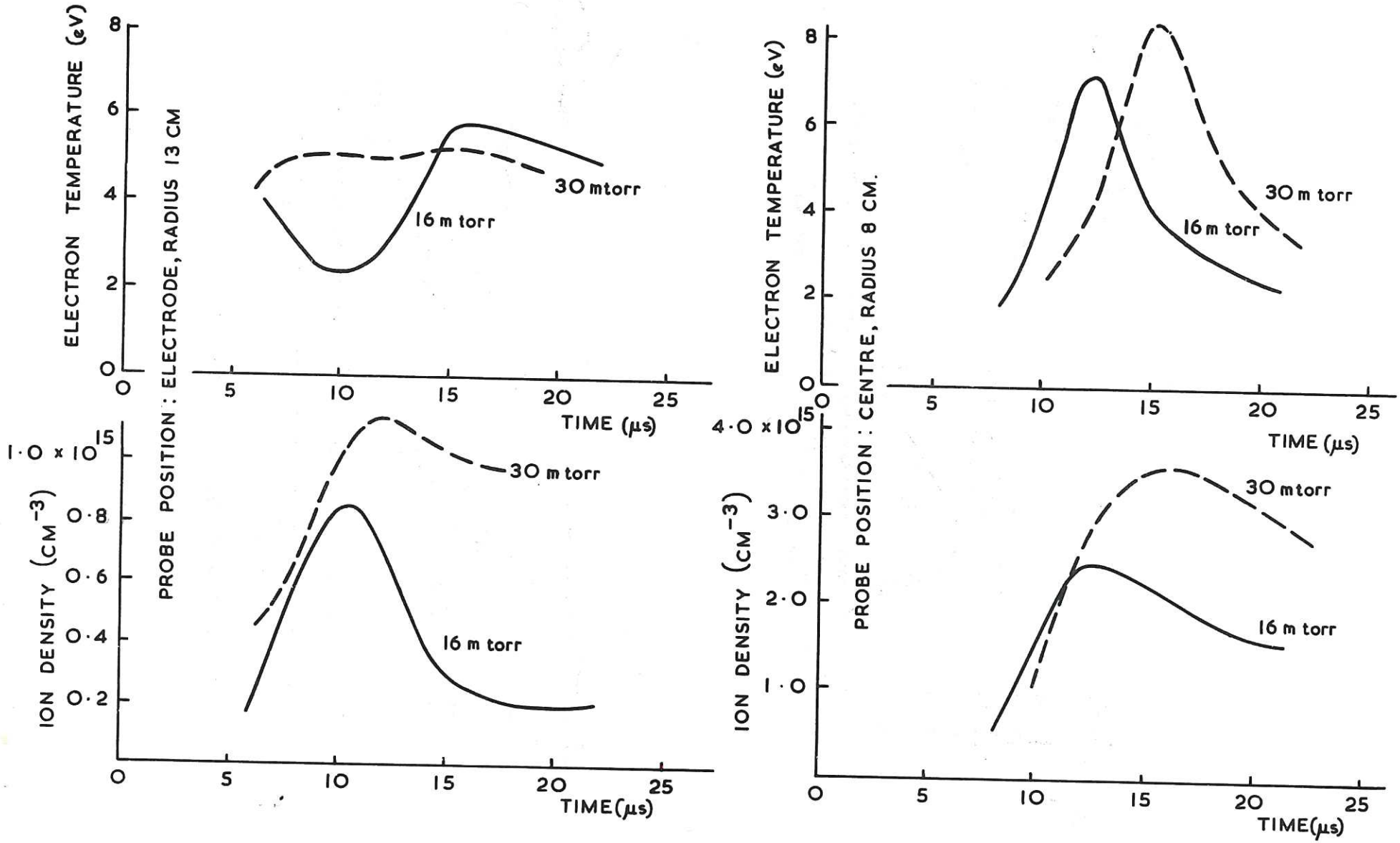

Fig. 26 Effect of pressure on density and temperature (CLM-P71)

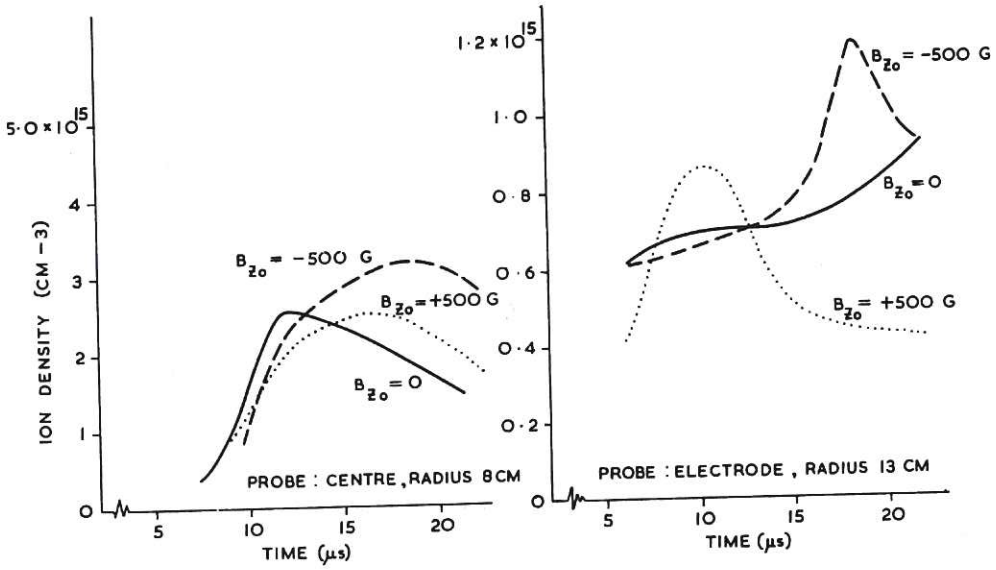

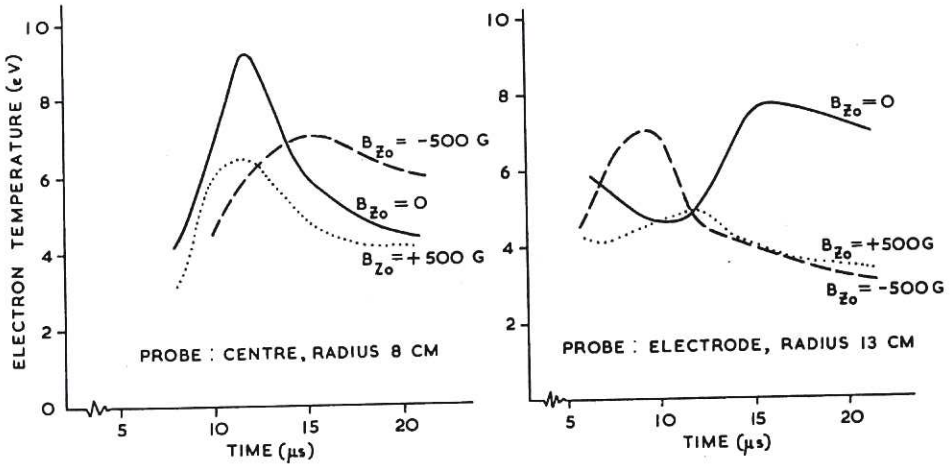

Fig. 27 Effect of B_{zo} on density and temperature (CLM-P71)

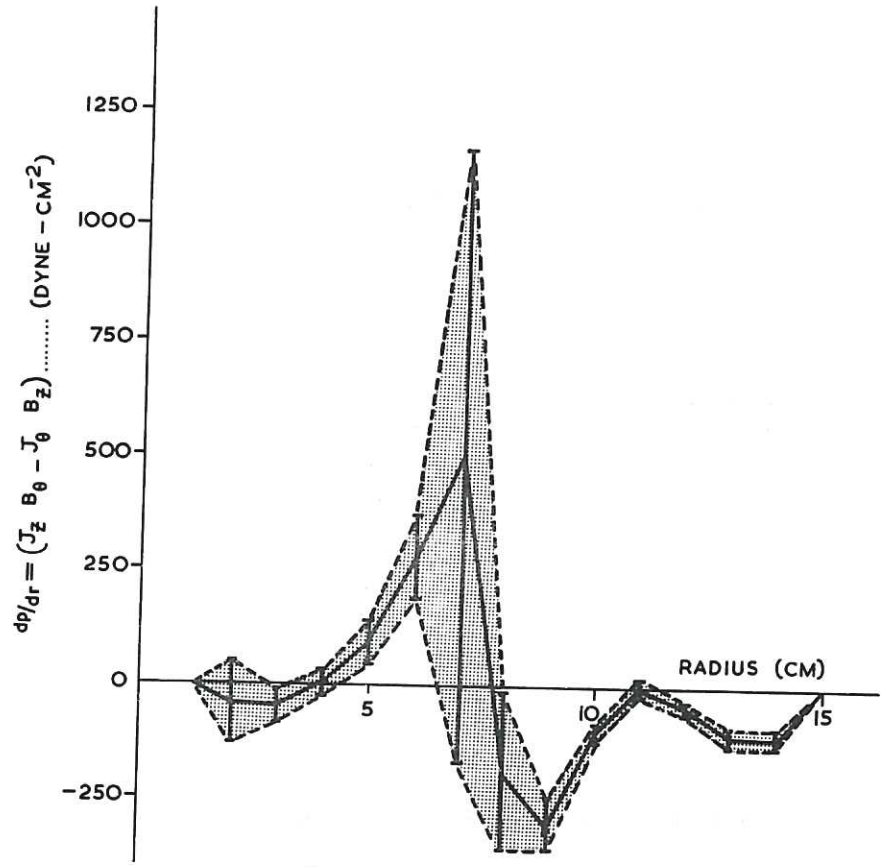

Fig. 28 $\frac{dp}{dr}$ at current maximum (CLM-P 71)

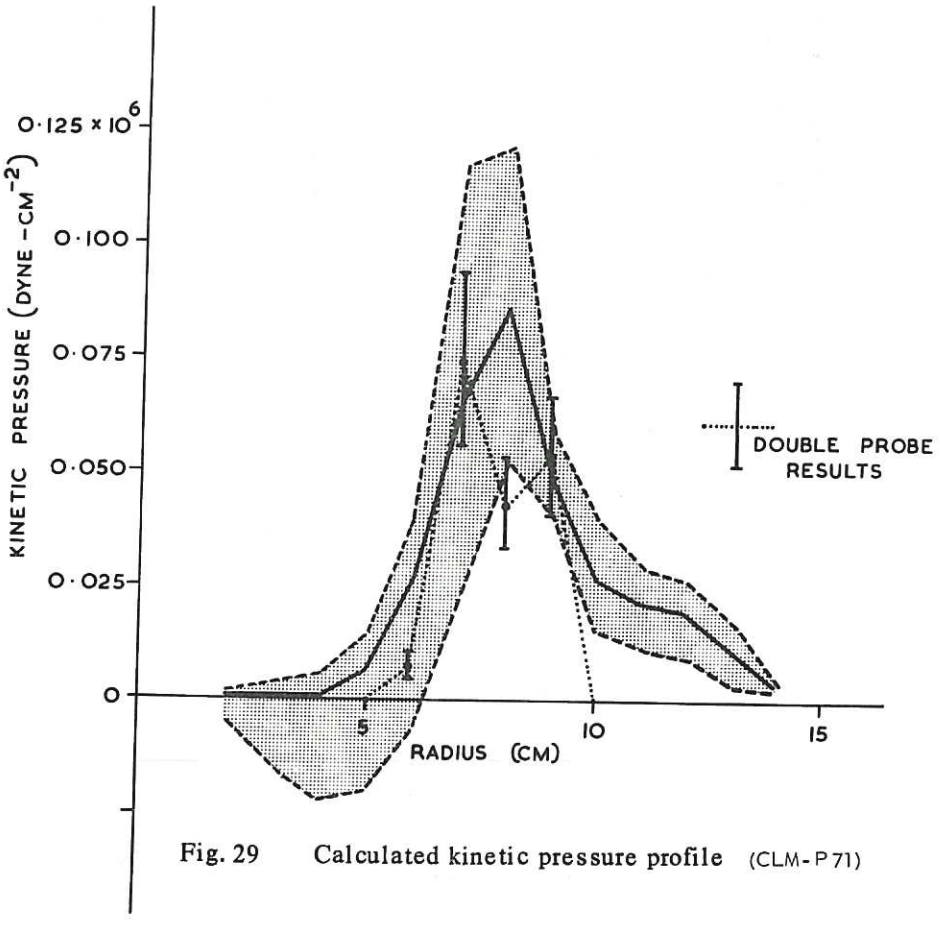

Fig. 29 Calculated kinetic pressure profile (CLM-P 71)

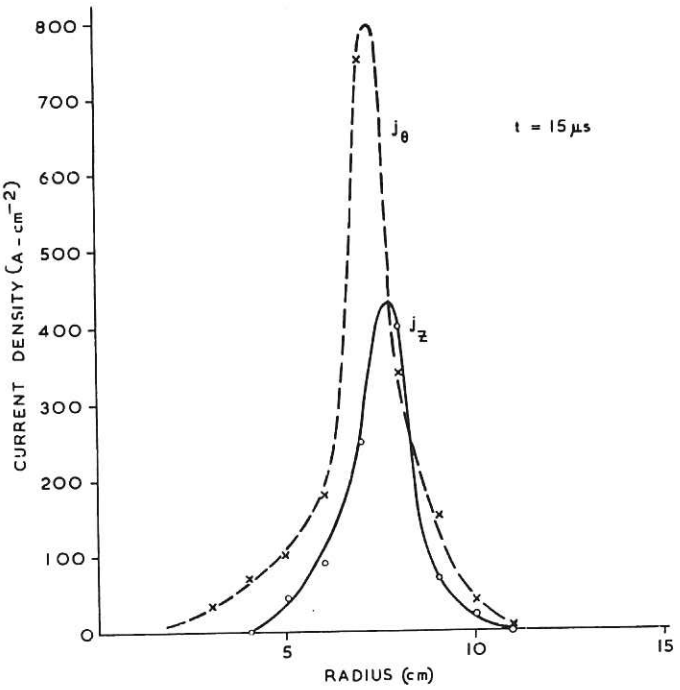

Fig. 30 Current density distributions (CLM-P71)

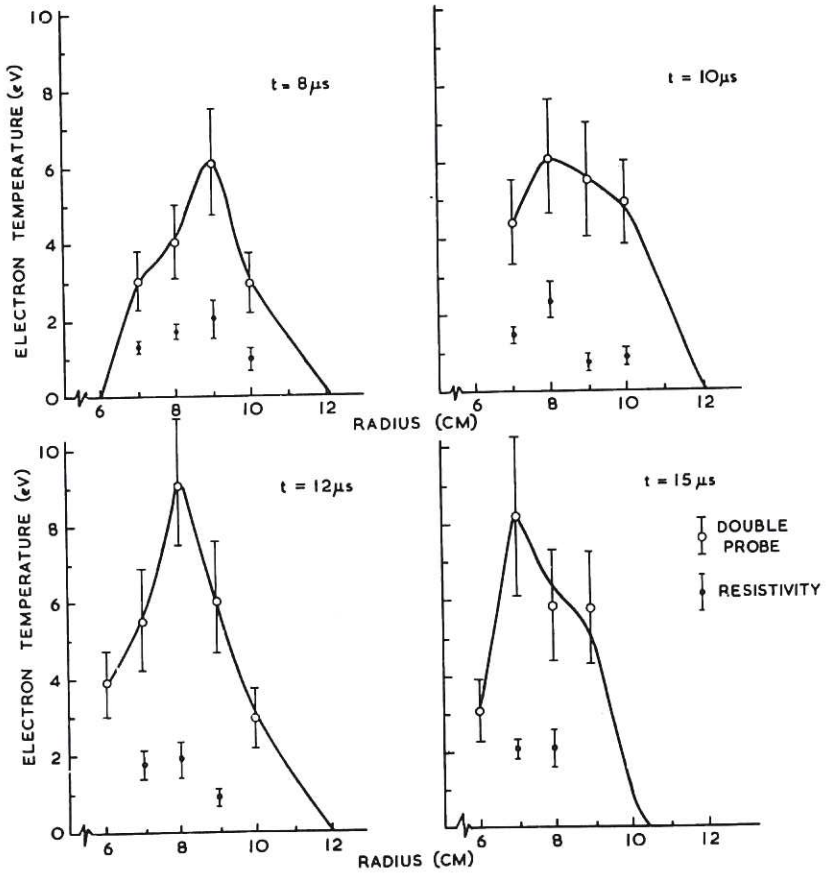

Fig. 31 (CLM-P71)
Comparison between double probe and resistivity electron temperature

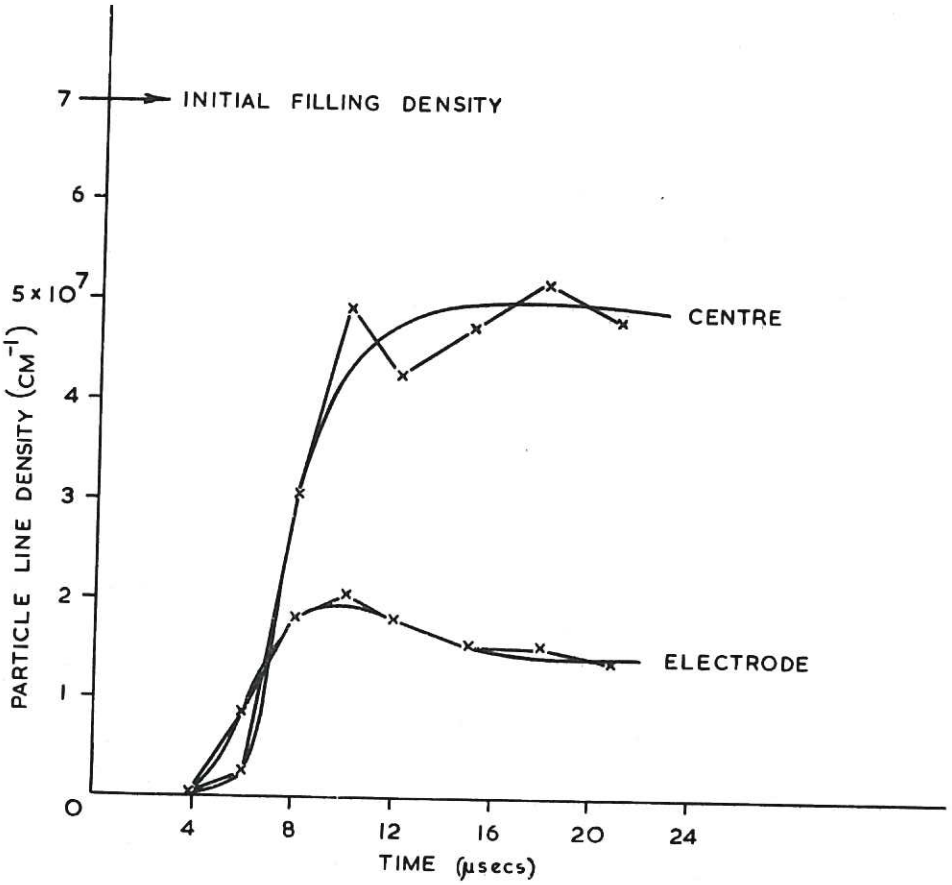

Fig. 32 Particle line densities (CLM-P 71)

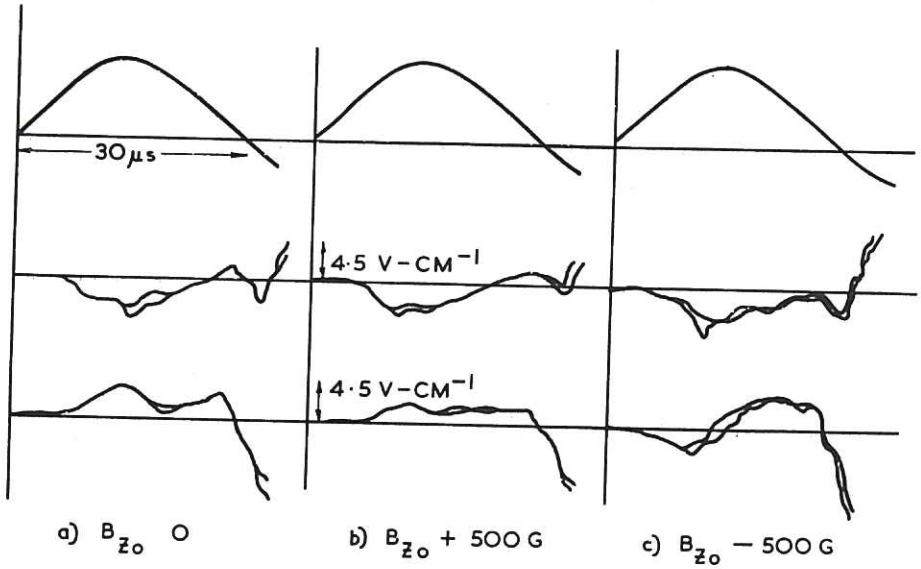

UPPER – APPLIED B_z FIELD

CENTRE – AZIMUTHAL ELECTRIC FIELD $-E_\theta$

LOWER – AXIAL ELECTRIC FIELD E_z

PROBE RADIUS 7 CM. CENTRE

Fig. 33 Electric field oscillograms (CLM-P 71)

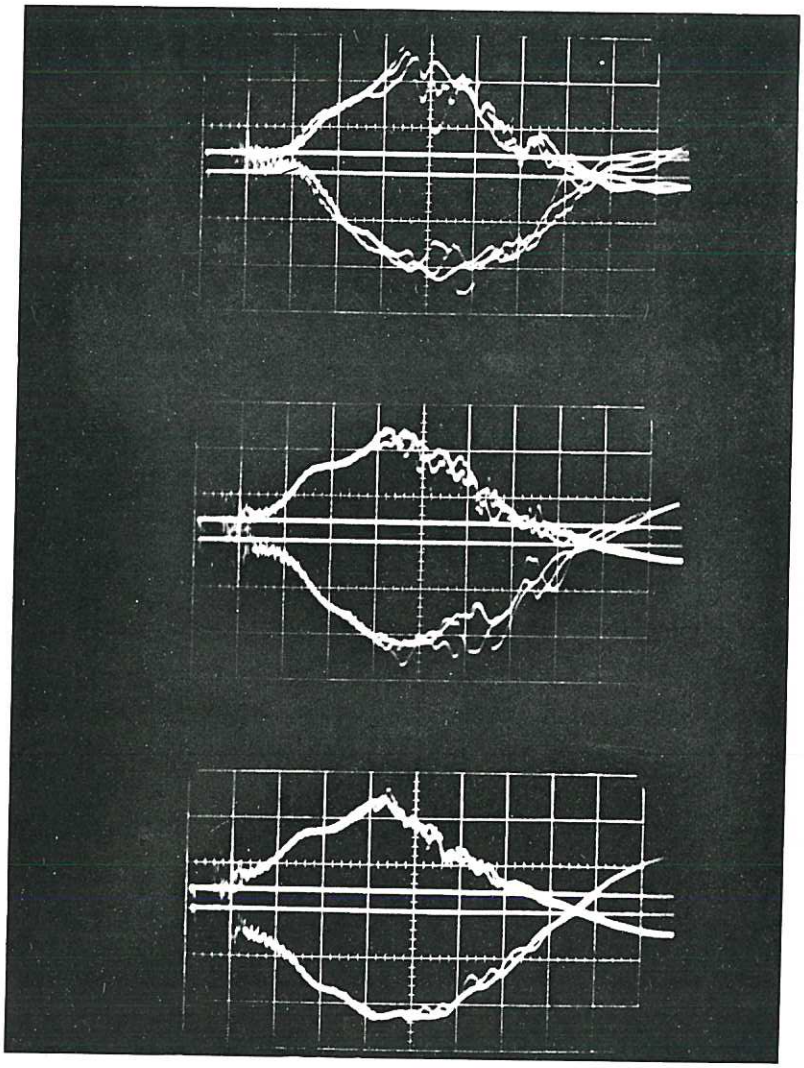

(a) $B_{zo} = -500$ G

(b) $B_{zo} = -200$ G

(c) $B_{zo} = 0$

Fig. 34 Superposed $\frac{dB_\theta}{dt}$ oscillograms (CLM-P 71)

Upper Trace - Probe Radius 9.1 cm
Lower Trace - Probe Radius 7.5 cm
3 shots per frame
Oscilloscope sweep 2 μs/cm